NO2 jet cooled visible excitation spectrum - Vibronic chaos induced by the X2A1-A2B2 interaction

A. Delon, R. Jost, M. Lombardi

NO_2 jet cooled visible excitation spectrum: Vibronic chaos induced by the $\tilde{X}\,^2A_1$–$\tilde{A}\,^2B_2$ interaction

A. Delon and R. Jost
Service National des Champs Intenses—C.N.R.S. BP 166X, 38042 Grenoble Cedex, France

M. Lombardi
Laboratoire de Spectrométrie Physique—U.J.F. BP 53X, 38402 Saint Martin d'Hères Cedex, France

(Received 16 April 1991; accepted 8 July 1991)

Significant improvements have been obtained on measurements of the NO_2 jet cooled excitation spectrum in the 16 300–18 502 cm^{-1} range, previously obtained by Smalley *et al.* [J. Chem. Phys. **63**, 4977 (1975)], Persch *et al.* [Ber. Bunsenges. Phys. Chem. **92**, 312 (1988)], and Hiraoka *et al.* [J. Mol. Spectrosc. **126**, 427 (1987)]. The improvements concern first the rotational analysis, owing to a better resolution (150 MHz) and absolute precision (500 MHz), and second the completeness and purity of the resulting vibronic sequence, owing to a better sensitivity. As a result, 159 vibronic energy levels have been observed in the 16 500–18 500 cm^{-1} energy range, where 210 ± 10 are expected. A detailed comparison with previous results is presented. The statistical analysis of the corresponding energy spacings shows that long range correlations up to 50 mean levels spacings are present, confirming the chaotic behavior of this set of vibronic levels. Furthermore, we analyze the observed rovibronic interactions (or rotational perturbations) that are responsible for the very irregular rotational behavior of the visible absorption spectrum of NO_2 at room temperature.

I. INTRODUCTION

During the last few years there were many attempts to observe experimentally the chaos lying in the vibrational degrees of freedom of polyatomic molecules. In quantum systems, chaos can be characterized by the existence of correlations among energy level spacings, which can be evidenced by the nearest neighbor distribution (NND), the long range correlation function $\Sigma^2(L)$ or $\Delta_3(L)$,[1] or by the Fourier transform of the unfolded spectrum.[1,2] Examples of significant experimental results were obtained with stimulated emission pumping (SEP) technique by Abramson *et al.*[3] on C_2H_2, and by Leviandier *et al.*[2] on methylglyoxal with an anticrossing technique.

However, all these experimental results suffer from lack of resolution and/or sensitivity, which do not allow one to get complete and pure sequences of vibrational energy levels. On the other hand, many numerical efforts both classical[4] (trajectories in phase space) and quantum mechanical (diagonalization of large matrices), have been devoted to the study of chaos in vibrations of polyatomic molecules. These numerical efforts are all basically limited by the quality of the potential energy surface (PES) and especially by the poor description of the vibrational mode couplings which play a crucial role. In polyatomic molecules, vibrational chaos is usually expected within the $3N$-6 (or $3N$-5) vibrational degrees of freedom of a given PES, usually those of the ground state. For triatomic molecules, like CO_2 or SO_2, the chaotic behavior is expected typically above 20 000 cm^{-1}.[5] For example, the vibrational spectrum of SO_2 is still regular at 21 000 cm^{-1}, or at least consists (at low resolution) of regular assignable "feature" states, as shown by Yamanouchi *et al.*[6]

For NO_2, on the contrary, there is a strong conical intersection between the $\tilde{X}\,^2A_1$ and $\tilde{A}\,^2B_2$ PES, which induces vibronic mixing (and consequently chaos) at much lower energy than expected solely within vibrational levels of the $\tilde{X}\,^2A_1$ PES.[7] In 1975, Smalley *et al.*[8] made decided experimental progress by using rotational cooling (down to 3 K) of a supersonic jet, which simplifies considerably the corresponding unassignable room temperature absorption or excitation spectrum. In the 14 880–17 518 cm^{-1} range, they have observed 140 vibronic bands (but only 114 true vibronic levels, see Sec. III B), i.e., much more than expected if the $\tilde{A}\,^2B_2$ state were involved alone. In 1985, Haller *et al.*[7] showed quantitatively with a model that the well-known complexity (and high line density) of the visible NO_2 absorption (or excitation) spectrum is due to this $\tilde{X}\,^2A_1$–$\tilde{A}\,^2B_2$ vibronic interaction. In 1988, Persch *et al.*[9] have extended the energy range of the jet cooled excitation spectrum from 12 117 cm^{-1} up to 24 563 cm^{-1}, but their list of 407 vibronic levels is rather inaccurate, except for some sequences of vibronic levels for which they have obtained a very high resolution spectrum ($\simeq$20 MHz) and assigned several rotational lines for each vibronic level.[10] At this level of resolution, the fine and hyperfine structures of both the upper and lower levels are resolved. The above mentioned model of $\tilde{X}\,^2A_1$–$\tilde{A}\,^2B_2$ vibronic interaction[7] is based on *ab initio* calculations of Jackels and Davidson,[11] and of Gillipsie *et al.*,[12] who predicted the $\tilde{A}\,^2B_2$ state at about 10 000 cm^{-1} above the $\tilde{X}\,^2A_1$ ground state and also predicted the corresponding $\tilde{X}\,^2A_1$–$\tilde{A}\,^2B_2$ conical intersection. However, *ab initio* calculations by Hirsch *et al.*[13] lead to a lower $\tilde{X}\,^2A_1$–$\tilde{A}\,^2B_2$ zero point energy separation of 7392 cm^{-1} and very recently Blahous *et al.*[14] have found an intermediate value of 8540

cm^{-1}. Elsewhere, we present the *complete* set of 191 lower vibrational levels (up to 10 000 cm^{-1}) observed in laser induced dispersed fluorescence spectra (LIDFS) from 11 upper vibronic levels located around 23 000 cm^{-1}.[15]

By extrapolation of these results to higher energies, we have been able to predict accurately the expected number of vibronic levels and then to determine the number of missing levels in the range of our excitation spectrum. In Sec. III we present a detailed analysis of the obtained jet cooled NO_2 excitation spectrum and we emphasize the comparison with previous results obtained by Smalley *et al.*[8], Persch *et al.*,[9] and Hiraoka *et al.*[16] in order to determine the best set of vibronic levels. In Sec. IV we analyze the irregularities of rotational level spacings and fine structure splittings due to *ro*vibronic interactions. It is important to note that these *ro*vibronic interactions do not induce vibronic chaos but induce only irregular rotational structures. In Sec. V we study the energy correlations within the observed set of vibronic levels given in Table II, we compare these correlations with those of the GOE standard model for quantum chaos, and we analyze the influence of missing levels.

II. EXPERIMENT

The experimental setup is similar to the one used for glyoxal.[17] A monomode ring dye laser (380A, Spectra Physics) pumped by an Ar^+ cw laser (171 or 2045 Spectra Physics) excite NO_2 molecules in a free jet about 2 mm from a 50 micron aperture nozzle. The NO_2 molecules (Air Liquide) are first condensed inside a tank, then carried along by an Argon flux at a total pressure of typically 1–3 bars. The concentration of NO_2, controlled by the temperature of the tank (-15 to -5 °C) is usually of the order of 1%. The vacuum chamber is evacuated by a 500 m^3/h root pump (Peiffer) and a 65 m^3/h mechanical pump (Alcatel). The corresponding back pressure is a few 10^{-2} Torr. The resulting NO_2 rotational temperature is about 3 K in the lowest $K=0$ ($N=0,2,4,...$) manifold. However, the vibrational temperature remains close to the room temperature and consequently hot bands have been observed. The fluorescence light is detected by a PMT at right angle to the jet and to the laser beam. In order to reduce the Doppler linewidth, an image of the fluorescence "flame" is observed through a slit perpendicular to the laser beam. The optimum slit (taking into account the resolution, the fluorescence intensity, and the scattered light) is trapezoidal, 4 mm long, and 0.4 mm of maximum width. The corresponding residual Doppler linewidth is less than 150 MHz, allowing resolution of the fine structures of the lower and upper rotational levels. Furthermore, a colored filter rejects the scattered laser light from the nozzle. Nevertheless, we have always observed a weak, but irreducible, spectrally continuous background of unknown origin in our NO_2 excitation spectra. The spectrum has first been obtained by juxtaposition of slightly overlapping 75 GHz scans. Then, the wavelength of each line suspected from its line shape to be R_0, P_2, R_2, P_4, etc. (see Sec. III) has been measured, with an eight digits homemade Lambdameter, to within 150 MHz (relative) and 500 MHz (absolute). During each measurement the laser frequency (slightly modulated) was locked onto the observed transition by a lock-in amplifier. The relative intensities of bands are given in Table II, only within 20%. Note that the weakest detected vibronic band is about 2000 times smaller than the strongest one!

III. EXCITATION SPECTRUM ANALYSIS

A. Rotational analysis and the vibronic band origins

Our band spectra appear similar to those published by Smalley *et al.*[8] (Figs. 2, 5, 6, 7, and 10). However, our better resolution allows for a finer rotational analysis because we are able to assign the fine structure J quantum numbers. Two examples of bands are shown in Figs. 1 and 2. First, NO_2 being almost a symmetric top, we use the N,K,J notation with the related A, $\overline{B}$ rotational constants. In the jet cooled excitation spectrum, we have only observed parallel type bands, i.e., $\Delta K=0$ rotational transitions. In addition, the low rotational temperature ($T_R \sim 3$ K) achieved in the supersonic beam expansion is such that the dominant transitions occur from $K=0$. Consequently, the more intense transitions of each vibronic band are the R_0, R_2, and P_2 ($K=0$) lines. The weak transitions, not analyzed here, belong mainly to the $K=1$ manifold. The $\tilde{X}\,^2A_1$ and $\tilde{A}\,^2B_2$ states being doublets, we observe the fine structure splittings (due to spin–orbit interactions) that are resolved in the ground state and are almost always resolved in the numerous upper states. Four independent criteria are used to assign rotational transitions:

(i) The R_0-P_2, R_2-P_4, and R_4-P_6 differences must correspond, within 150 MHz, to the ground state splittings of, respectively, 2.532 cm^{-1}, 5.908 cm^{-1}, and 9.280 cm^{-1} between $N''=0$ and $N''=2$ ($6\ \overline{B''}$), $N''=2$ and $N''=4$ ($14\ \overline{B''}$), and $N''=4$ and $N''=6$ ($22\ \overline{B''}$).

(ii) The R_0-P_2, R_2-P_4, and R_4-P_6 lines have reproducible and stable intensity ratios at a given rotational temperature (about 3 K).

(iii) Fine structure splittings of the $N'=1$, 3, etc. excited levels must be the same (within 150 MHz) when observed on the R_0 or on the P_2 lines for $N'=1$, on R_2 and P_4 for $N'=3$, and so on.

(iv) The high resolution profile of each fine structure component ($J'=N'\mp 1/2$) allows us to identify these two components because these two high resolution profiles are very different (see Ref. 10).

It is therefore possible, on the basis of these four criteria, to assign rotationally the observed transitions, i.e., upper levels, and subsequently, to build up the corresponding upper vibronic excited states. Several pieces of information can therefore be obtained on each vibronic level as given in detail in Table I [Ref. 18(a)] and summarized in Table II.

(i) The R_0-P_2 and R_2-P_4 fine structure splittings allow one to obtain the value of the fine structure "constant," if one assumes that the fine structure splitting is given by

$$E_{N'}(J'=N'+\tfrac{1}{2})-E_{N'}(J'=N'-\tfrac{1}{2}) = \tfrac{1}{2}\bar{\epsilon}(2N'+1), \quad (1)$$

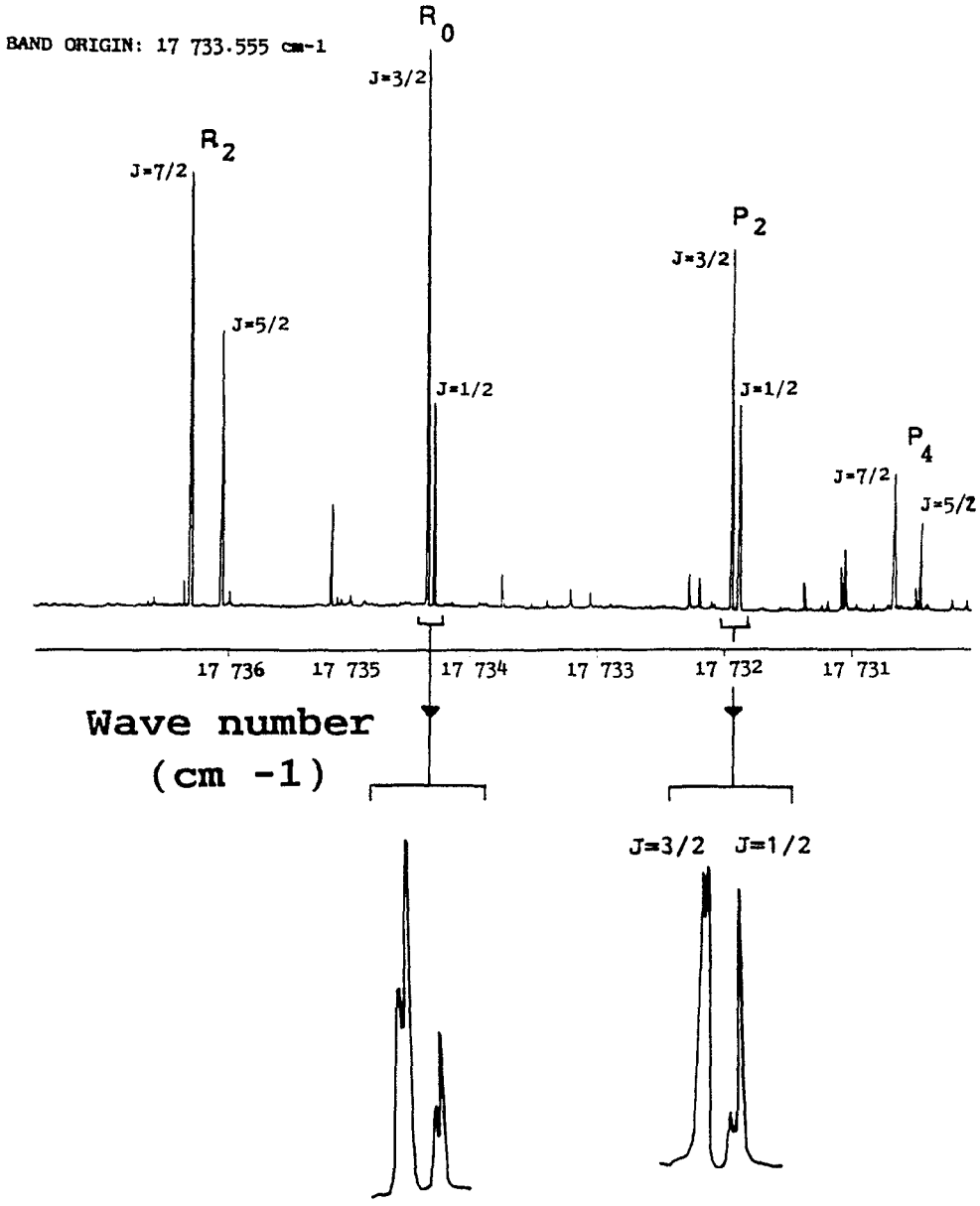

FIG. 1. Example of a normal band (top): each rotational component is split into two fine structure components ($J = N \mp 1/2$). Weak lines are $K \neq 0$ transitions. High resolution measurements (bottom) allow us to identify the J fine structure components according to the individual line shapes.

where $\overline{\epsilon'} = (\epsilon'_{bb} + \epsilon'_{cc})/2$. In fact, it very often appears that the value of $\overline{\epsilon'}$ for $N' = 1$ (from R_0 or P_2 lines) is not the same as that for $N' = 3$ (from R_2 or P_4 lines)! This fact has already been reported[10,19,20] but without further analysis. We present in Sec. IV a statistical analysis of this phenomenon as well as a physical interpretation.

(ii) From the barycenters of the two fine structure components of the $N' = 1, N' = 3$, and $N' = 5$ rotational levels, it is then possible to obtain $\overline{B}'_{1,3}$ and $\overline{B}'_{3,5}$, the "local" rotational constants, corresponding to the $E(N' = 3) - E(N' = 1)$ and $E(N' = 5) - E(N' = 3)$ energy differences. Once again it appears very often that the value of the $\overline{B'}$ rotational constant is not the same when calculated, respectively, from $N' = 3$ and $N' = 1$ levels or from $N' = 5$ and $N' = 3$ levels. This point is discussed in Sec. IV.

(iii) Last but not least, among the 166 observed vibronic bands from 16 319 cm^{-1} to 18 502 cm^{-1}, 57 display extra lines in the $K = 0$ manifold corresponding to $N' = 1$ and/or $N' = 3$ and/or $N' = 5$, as indicated in the last column of Table II. More precisely, we have observed bands with more than two pairs of $R_0 - P_2$ and/or $R_2 - P_4$ and/or $R_4 - P_6$ lines separated, respectively, by 2.532, 5.908, and 9.280 cm^{-1} energy splittings. Figure 2 displays one of these bands with a $R_0 - P_2$ pair of $J = 3/2$ extra lines. These three pairs of lines correspond to the existence of three fine structure levels in the $N' = 1$ upper level. In the case of three $R_0 - P_2$ lines, the three corresponding J quantum numbers are either

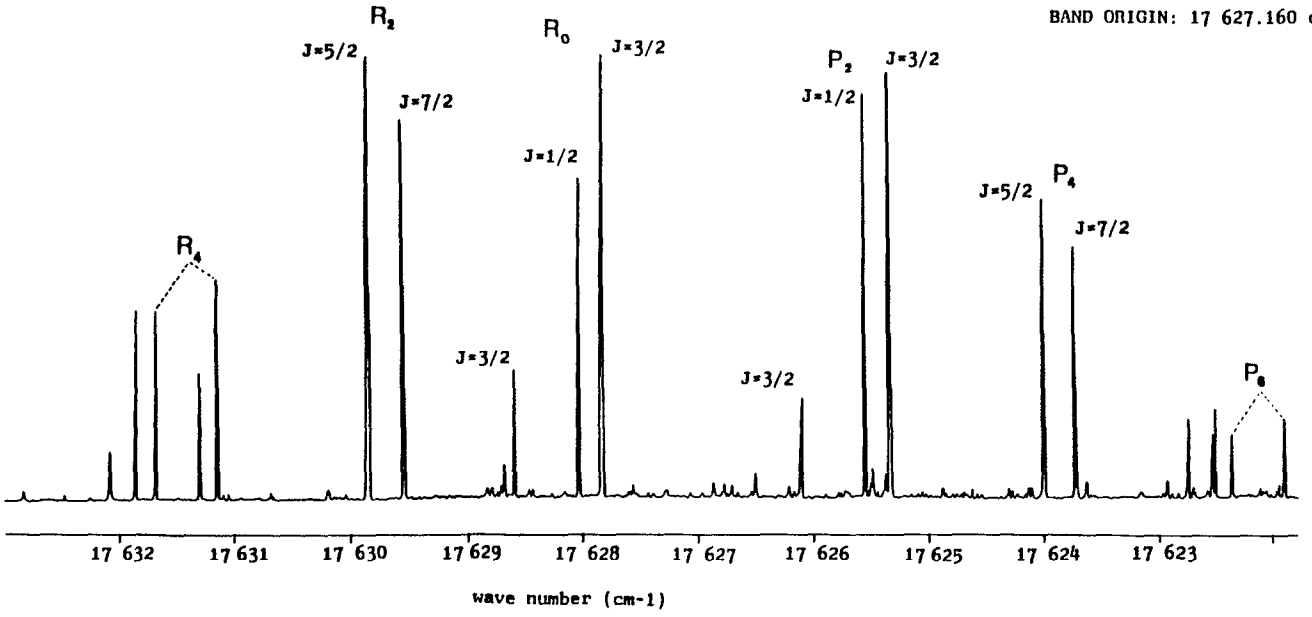

FIG. 2. Example of a band with a pair of $J = 3/2$ "extra" lines: R_0 and P_2 transitions, which display three fine structure components: one $J = 1/2$ and two $J = 3/2$.

TABLE II. Energy, fine structure splittings, and rotational constants of 166 $^2B_2$ vibronic levels. All energies are given in cm^{-1}.

Relative intensities[a]	B.O.[b]	FS ($N=1$)[c] 3/2-1/2	FS ($N=3$)[c] 7/2-5/2	$B_{1,3}$[d]	$B_{3,5}$[d]	Extra lines[e] j1 = 1/2 j2 = 3/2 j3 = 5/2 j4 = 7/2
4.0	16 319.136	0.000	− 0.304	0.3779		
40.0	16 321.136	+ 0.316	+ 0.465	0.4737		j2
1.0	16 337.023	− 0.120	+ 0.130	0.4001		
0.6	16 361.734	0.000	− 0.036	0.3989	0.4036	
2.0	16 413.944	+ 0.105	+ 0.180	0.4363	0.4216	
13.0	16 436.065	+ 0.039	+ 0.146	0.4203	0.4234	
1.0	16 449.728	+ 0.381	+ 0.256	0.4192		j2
3.5	16 501.887	+ 0.075	− 0.010	0.4032	0.4078	j2
4.0	16 511.414	− 0.333	− 0.466	0.3552	0.3668	j2
6.7	16 577.887	+ 0.103	+ 0.456	0.3757	0.4377	
11.0	16 602.469	+ 0.249	+ 0.558	0.4401	0.4354	
4.0	16 615.125	+ 0.039	+ 0.084	0.4143	0.4246	
10.0	16 631.274	+ 0.080	+ 0.150	0.4264	0.4293	
5.0	16 643.355	+ 0.145	+ 0.343	0.4134	0.3997	
1.7	16 651.341	− 0.668	− 0.982	0.3990		
6.8	16 657.456	+ 0.052	+ 0.231	0.3470	0.3789	j2
6.4	16 658.204	+ 0.757	+ 0.882	0.4813	0.4363	
3.3	16 671.675	+ 0.033	+ 0.072	0.4137	0.4094	
1.6	16 692.890	0.000	0.000	0.4155		
3.6	16 704.128	+ 0.034	+ 0.137	0.4253	0.4149	
0.25	16 710.846	+ 1.035	0.000	0.4390		
1.6	16 713.745	+ 0.050	− 0.209	0.4306		
12.0	16 728.366	0.000	+ 0.043	0.4132	0.4153	
17.0	16 757.795	0.000	+ 0.052	0.3636	0.3697	
3.7	16 770.564	+ 0.092	+ 0.202	0.4462	0.4236	
0.6	16 786.109	− 0.383	− 0.162	0.4169	0.3989	
1.4	16 798.696	+ 0.018	0.000	0.3993	0.3961	
9.0	16 809.976	− 0.225	− 0.854	0.4321		j1
3.8	16 837.782	+ 0.033	+ 0.150	0.4217	0.4094	
100.0	16 849.462	− 0.070	− 0.161	0.4239	0.4203	
2.9	16 868.300	+ 0.066	+ 0.045	0.4152		
10.0	16 875.171	− 0.017	− 0.047	0.4051	0.4025	
17.5	16 885.080	+ 0.408	− 0.608	0.3642		
25.0	16 893.147	+ 0.080	+ 0.108	0.4120	0.4212	j4
2.9	16 909.603	+ 0.094	+ 0.019	0.4089	0.4157	
2.9	16 917.082	− 0.144	− 0.130	0.4163	0.4186	
7.0	16 927.802	+ 0.086	+ 0.164	0.4276	0.4200	

TABLE II. (*Continued.*)

Relative intensities[a]	B.O.[b]	FS ($N=1$)[c] 3/2-1/2	FS ($N=3$)[c] 7/2-5/2	$B_{1,3}$[d]	$B_{3,5}$[d]	Extra lines[e] j1 = 1/2 j2 = 3/2 j3 = 5/2 j4 = 7/2
16.0	16 946.711	−0.322	−0.668	0.4153	0.4118	
0.2	16 967.170	−0.306	−0.178	0.4175		j1
7.0	16 975.537	−0.013	+0.094	0.4203	0.4050	j1 j4
21.0	17 001.785	+0.093	+0.301	0.4091	0.3958	
9.0	17 009.956	+0.172	−0.279	0.4526	0.4483	
70.0	17 027.534	−0.023	−0.096	0.4212	0.4226	j3
7.5	17 043.961	−0.264	−0.430	0.4089		j3
5.0	17 061.475	−0.059	−0.175	0.3929		
68.0	17 092.066	+0.033	−0.107	0.4087	0.4642	j4
1.9	17 101.539	+0.059	+0.220	0.4118		
9.5	17 116.070	−0.099	0.000	0.3637		
11.0	17 116 965	−0.209	+0.508	0.3979	0.4009	j3
1.0	17 129.949	−0.007	+0.268	0.3931		
1.0	17 142.252	+0.128	+0.295	0.4225	0.4148	
3.5	17 159.592	0.000	−0.187	0.4299		j1 j3
1.4	17 182.214	+0.051	−0.182	0.4084		
4.0	17 209.861	+0.086	+0.203	0.4329	0.4285	
8.7	17 219.264	−0.006	+0.116	0.4349	0.4459	j2 j4 j4
2.0	17 254.513	−0.020	−0.091	0.4251		j2 j4
17.5	17 257.767	+0.031	+0.084	0.4007	0.3996	
10.0	17 266.578	−0.012	+0.053	0.3852	0.3961	j3
18.0	17 280.760	−0.295	−0.217	0.4061	0.3969	j2
3.3	17 297.630	−0.472	+0.728	0.4927		j2
1.2	17 306.867	+0.244	−0.325	0.4487		
1.7	17 312.924	−0.620	+0.156	0.4357	0.3883	
1.0	17 317.653	−0.144	−0.146	0.3832		
1.0	17 331.726	−0.162	−0.443	0.3816	0.3800	
1.0	17 348.285	+0.013	+0.217	0.4084		
0.1	17 358.648	+0.267	+0.594	0.4062		
8.0	17 376.010	0.000	−0.031	0.3751	0.3764	
30.0	17 382.002	−0.219	−0.245	0.4084	0.4067	
5.0	17 400.769	+0.388	+0.090	0.4045	0.4296	j4
2.0	17 410.420	+0.067	+0.177	0.4047		
5.0	17 412.957	−0.041	0.000	0.3873		
10.0	17 431.205	+0.036	+0.162	0.4149		
30.0	17 437.060	0.000	+0.078	0.4117	0.4092	
4.0	17 455.594	−0.902	−1.220	0.3869		
4.0	17 466.853	+0.054	+0.043	0.4000		
60.0	17 477.640	+0.390	+0.835	0.4252		j4
45.0	17 491.874	−0.055	+0.434	0.4253		j1
9.0	17 519.189	−0.084	−0.253	0.3742		j4
80.0	17 528.127	+0.366	+0.902	0.4665	0.4603	
5.0	17 534.360	−0.290	+0.197	0.3700		j2 j4
14.0	17 551.260	+0.244	−1.094	0.4528		
15.0	17 553.602	+0.990	0.000	0.4877		
14.0	17 576.903	−0.186	−0.296	0.3666		
0.6	17 579.887	−0.112	−0.091	0.3951		
9.0	17 591.662	−0.642	−1.412	0.4029		
13.0	17 595.122	+0.450	−1.225	0.4856		
15.0	17 601.469	−0.334	−0.129	0.4019		
35.0	17 606.872	−0.755	+0.260	0.4558		j2
15.0	17 615.355	−0.519	−0.723	0.4044		
45.0	17 627.160	+0.051	−0.276	0.4261	0.4201	j2
3.0	17 647.828	+0.014	+0.024	0.3887		
10.0	17 668.798	+0.080	+0.300	0.4045		
15.0	17 675.373	+0.142	+0.102	0.4084		
20.0	17 679.025	−0.022	+0.054	0.4355		
75.0	17 684.494	+0.226	+0.304	0.4375		
15.0	17 700.080	+0.037	+0.084	0.4002		
60.0	17 713.203	+0.128	+0.137	0.3775	0.4173	
120.0	17 721.875	−0.147	−0.364	0.4137	0.4157	
65.0	17 733.555	+0.080	+0.244	0.4362		
12.0	17 749.872	−0.163	−0.304	0.3946		j1
1.4	17 768.491	+0.132	+0.248	0.4141		
2.5	17 776.717	−0.038	−0.366	0.4021		
4.5	17 786.878	0.000	+0.078	0.4072		
6.0	17 795.345	−0.117	−0.045	0.4433		j2
28.0	17 812.624	−0.040	+0.058	0.3882		j2

TABLE II. (*Continued.*)

Relative intensities[a]	B.O.[b]	FS ($N=1$)[c] 3/2-1/2	FS ($N=3$)[c] 7/2-5/2	$B_{1,3}$[d]	$B_{3,5}$[d]	Extra lines[e] j1 = 1/2 j2 = 3/2 j3 = 5/2 j4 = 7/2
8.0	17 814.257	− 0.146	− 0.262	0.4142		
5.0	17 833.060	+ 0.264	+ 0.332	0.4261		
100.0	17 842.578	− 0.158	− 0.325	0.4024	0.4345	
30.0	17 843.666	+ 0.024	+ 0.027	0.4103	0.4126	j3
11.0	17 855.296	+ 0.305	− 0.284	0.3632		j2
40.0	17 874.425	+ 0.150	+ 0.257	0.4530		
35.0	17 892.302	+ 0.099	+ 0.127	0.4182		j2
7.0	17 897.835	+ 0.010	+ 0.046	0.4112		
50.0	17 907.832	− 0.513	− 0.236	0.3517		j4
8.0	17 929.193	0.000	+ 1.330	0.4527	0.4721	j1
8.0	17 941.716	+ 0.322	+ 0.226	0.4019		
6.0	17 943.412	− 0.230	− 0.448	0.3978		
15.0	17 960.405	− 0.012	− 0.017	0.4056		
40.0	17 970.246	0.000	− 0.016	0.4171	0.4172	
11.0	17 997.085	− 0.013	+ 0.348	0.3936	0.4056	j2 j3 j4
16.0	18 022.467	+ 0.054	+ 0.055	0.3756	0.3758	
45.0	18 025.867	+ 0.083	+ 0.272	0.4748	0.4333	j3 j3
32.0	18 035.524	− 0.217	− 0.508	0.3924		j2 j3
7.0	18 041.443	+ 0.106	+ 0.064	0.4082		j2
38.0	18 056.318	− 0.086	+ 0.046	0.4429	0.4340	j1
95.0	18 073.013	− 0.184	− 1.160	0.4150	0.3873	
40.0	18 075.078	+ 0.607	− 0.354	0.4588		
60.0	18 078.734	− 0.543	− 1.272	0.3738		j1
36.0	18 095.411	+ 0.327	+ 0.752	0.3883	0.3904	
9.0	18 114.413	− 0.204	− 0.340	0.3917		
55.0	18 120.483	+ 0.056	+ 0.134	0.4003	0.4146	
12.0	18 132.990	+ 0.452	− 0.015	0.4400	0.4167	j1
10.0	18 142.745	+ 0.029	− 0.196	0.4337		
20.0	18 146.172	+ 0.040	+ 0.100	0.4024	0.4018	
11.0	18 152.786	− 0.044	− 0.124	0.4000		
4.0	18 171.491	+ 0.090	0.000	0.4241	0.4153	
125.0	18 199.165	− 0.237	− 1.050	0.3959	0.4273	j2
36.0	18 207.803	+ 0.104	+ 0.016	0.4630		
24.0	18 212.237	+ 0.158	+ 0.318	0.4494	0.4389	
10.0	18 224.067	− 0.278	− 0.920	0.3678		
26.0	18 244.235	− 0.090	+ 0.284	0.3918	0.4003	
21.0	18 249.158	+ 0.093	− 0.029	0.4330	0.4177	j3 j4
68.0	18 265.357	− 0.031	+ 0.166	0.3983	0.3609	j2 j4
127.0	18 273.462	+ 0.154	+ 0.294	0.4295	0.4142	
60.0	18 280.551	+ 0.035	− 0.105	0.4465	0.4237	j2 j4
9.0	18 285.764	+ 0.059	+ 0.147	0.3861		j3 j4
100.0	18 304.093	− 0.074	− 0.160	0.4186	0.4067	j4
40.0	18 322.735	+ 0.085	+ 0.220	0.4094		
14.0	18 330.362	+ 0.720	− 1.337	0.2574		
23.0	18 347.776	+ 0.367	− 0.487	0.4970		j4
24.0	18 351.788	− 0.135	− 0.121	0.4349		
8.0	18 361.805	− 0.326	− 1.795	0.5637		j4
8.0	18 372.107	− 0.081	− 0.184	0.3965	0.3998	
100.0	18 383.255	+ 0.038	− 0.092	0.4220	0.4273	j3
35.0	18 397.925	− 0.230	− 0.809	0.4208	0.4328	j1 j2 j2 j3
64.0	18 412.457	+ 0.068	+ 0.147	0.4093	0.3995	
11.0	18 416.237	+ 0.020	− 0.167	0.3638		j2
37.0	18 424.383	+ 0.326	− 0.524	0.4577	0.4440	j2 j2
53.0	18 426.788	+ 0.786	+ 2.192	0.4783		j1 j2
19.0	18 438.930	− 0.490	− 0.356	0.3737		
190.0	18 447.813	− 0.006	− 0.131	0.3686	0.3810	j1 j2
8.0	18 467.480	− 0.027	− 1.018	0.3403		j1 j2
3.0	18 469.370	− 0.234	− 0.270	0.5254		
10.0	18 472.090	+ 0.442	+ 1.165	0.4539	0.4432	j4
1.5	18 484.677	+ 0.070	+ 0.165	0.4046		
3.2	18 502.192	+ 0.123	+ 0.372	0.3832		

[a] Relative intensities are given to ∓ 20%.
[b] Vibronic band origins.
[c] Fine structure splittings for $N=1$ and $N=3$.
[d] Calculated rotational constants from the spacings between $N=1$, $N=3$ ($B_{1,3}$) and between $N=3$, $N=5$ ($B_{3,5}$).
[e] "Extra" lines, when observed, are labeled according to their high resolution signature.

two $J = 1/2$ and one $J = 3/2$ or the opposite, indicating that either the $J = 1/2$ or the $J = 3/2$ fine structure level is split into two components by a *ro*vibronic interaction. As a whole, we have observed 14 "extra" levels with $J = 1/2$ and 30 with $J = 3/2$ on the $N' = 1, K = 0$ manifold, and 14 with $J = 5/2$ and 20 with $J = 7/2$ in the $N' = 3, K = 0$ manifold. We have conducted an exhaustive search for $J' = 1/2$ and $J' = 3/2$ extra lines and are therefore confident in the 14/30 ratio between the numbers of $J' = 1/2$ and $J' = 3/2$ extra lines. This important result will be discussed in Sec. IV. We want to emphasize that these extra lines have not been clearly assigned previously, leading to spurious vibronic levels as discussed in Sec. III B. Furthermore, when one extra line is observed, it is possible, on the basis of the energy shift and intensity ratios, to "deperturb" these pairs of levels and then to obtain the corresponding deperturbed energy levels. These "deperturbed" energy levels have been used to calculate the above mentioned rotational and fine structure constants. The J values of extra levels are given in the last column of Table II.

(iv) Finally, we have determined (by subtracting $2\overline{B}'_{1,3}$ from the observed $N' = 1$ energy level) the vibronic energy of each vibronic band.

The corresponding results on the 166 observed vibronic bands are given in Table I and summarized in Table II.

Hot bands with the $(0,n_2 = 1,0)$ vibrational level of the ground state as lower level have also been detected. Three independent criteria have been used to assign the hot bands lying between 16 319 and 17 752 cm^{-1} (= 18 502–749.65 cm^{-1}). Obviously, we cannot assign hot bands that occur in the 17 752–18 502 cm^{-1} energy range. For each hot band, a parent cold band, originating from the vibrationless level of $\tilde{X}\,^2A_1$, and then shifted by 749.65 cm^{-1}, must be found above in the excitation spectrum within 0.02 cm^{-1} with an intensity 75 times stronger in average ($T_{vib} = 260$ K, see below). In addition, the parent band must display the same rotational and fine structure splittings as the hot band within 0.005 cm^{-1}. The probability for these criteria to be satisfied simultaneously while the suspected band is not a hot band is extremely low. The list of the nine detected hot bands is given in Table III. The 260 K vibrational temperature, estimated from the hot band to cold band intensity ratios, is not significantly lower than room temperature, indicating that the vibrational degrees of freedom are not efficiently cooled in our jet conditions as previously observed.[4,21]

TABLE III. Listing of identified hot bands and of corresponding parent cold bands.

$T_v(H)$ Hot band origins (cm^{-1})	$T_v(P)$ Parent cold band origins (cm^{-1})	$T_v(P)-T_v(H)$ (cm^{-1})	Intensity ratio $I(P)/I(H)$
16 342.429	17 092.066	749.637	39
16 531.103	17 280.760	749.657	45
16 727.964	17 477.640	749.676	100
16 778.458	17 528.127	749.669	133
17 323.361	18 073.013	749.652	48
17 345.781	18 095.411	749.630	30
17 370.848	18 120.483	749.635	69
17 573.085	18 322.735	749.650	160
17 633.605	18 383.755	749.650	50

B. Comparison with previous results

In Table IV [Ref. 18(b)] we have compared our results with those obtained by Smalley *et al.*,[8] Persch *et al.*,[9] and Hiraoka *et al.*[16]

1. Comparison with Smalley's results

In the 16 319–17 492 cm^{-1} portion of the energy range common to our own present measurements and to the work of Smalley *et al.* (Table I of Ref. 8), they have observed 65 vibronic bands, among which two are given as hot bands in Table II of Ref. 8. Furthermore, we have found that bands number 108 and 130 in Table I of Ref. 8 should also be assigned as hot bands because we have observed the two corresponding cold bands (above 17 492 cm^{-1}, the maximum energy observed by Smalley). These two hot bands are listed in our hot bands (Table III). Moreover, we have reinterpreted a few pairs of their bands, almost degenerate in energy, as single bands including one (or a few) extra line(s): Bands number 120 and 121 in Smalley's Table I should be considered as one, the band given at 17 159.592 cm^{-1} in our Table II. This band has two extra lines, as quoted in the last column of Table II. Similarly, the two bands number 124 and 125 of Smalley's Table I should be grouped into one band at 17 219.264 cm^{-1} with three extra lines (see Table II). Last but not least, we have found, in our common energy range, 17 new vibronic cold bands, mostly with low intensities. As a result, we have observed a total of 77 cold bands (i.e., vibronic levels) in the 16 319–17 492 cm^{-1} common energy range, while Smalley *et al.*[8] have observed 56 of them. Globally, the agreement between Smalley's and our energy measurements is satisfactory: their vibronic energies are globally shifted by only 0.27 cm^{-1} with respect to ours, and the corresponding rms deviation is only 0.13 cm^{-1}. Among the 140 vibronic bands given by Smalley *et al.* (Ref. 8, Table I), we conclude that 114 are true cold vibronic bands, i.e., vibronic levels. In addition, we note that, due to a limited resolution ($\simeq 1$ GHz), Smalley *et al.* could not assign the fine structure component (i.e., the J values) and consequently could not determine the sign of the fine structure.

2. Comparison with Persch's results

Persch's results (2) are of inhomogeneous quality.

(i) Part of their measurements have been obtained at very high resolution (15 MHz) and are reported with a 10^{-3} cm^{-1} resolution in their Table I. These high resolution results, when compared with our line measurements, agree very well with our results: a mean shift of 0.013 cm^{-1} and a standard deviation of 0.032 cm^{-1}. However, there exist a few discrepancies in the detailed rotational analysis of the two vibronic levels at 16 899.200 and 17 078.200 cm^{-1}.

(ii) Most of their vibronic bands have been obtained from a low resolution spectrum, i.e., without detailed rota-

tional analysis and measurement (their analysis is based on a shape recognition technique of parallel bands).

In their low resolution spectrum, we have considered separately the energy range studied previously by Smalley *et al.*[8] and the range not studied by these authors. For the energy range previously known, their vibronic energies are in reasonable agreement with ours and Smalley's: when we compare the energies of 61 vibronic levels, we find a mean shift of 0.05 cm^{-1} and a standard deviation of 0.6 cm^{-1}. Moreover, they considered as cold bands those assigned as hot bands by Smalley *et al.*[8] in their Table II. When one considers the range 17 500–18 502 cm^{-1}, not studied previously by Smalley (containing 46 vibronic bands), one finds a standard deviation of 3.5 cm^{-1}. Considering that the mean vibronic energy level spacing is ~ 12 cm^{-1}, this 3.5 cm^{-1} deviation means that Persch's vibronic band origins are randomly distributed when compared with our own set of vibronic energy levels! Furthermore, other similar comparisons with our measurements (not reported here) in the 21 733–23 650 cm^{-1} range have been performed on a set of 53 vibronic levels given in Table I of Ref. 9. Again we come to the conclusion that there are no correlations between their values and ours. We conclude that very many band origins in the range not previously published by Smalley *et al.*,[8] given within a claimed accuracy of 0.1 cm^{-1} in Table I of Ref. 9, are not meaningful. We conclude that, among the 141 vibronic levels taken into account in the statistical analysis by Zimmermann *et al.*,[22] there are 25 spurious levels, among which 22 come from hot bands (most of them being listed in Smalley's Table II, Ref. 8), and three correspond to spurious bands due to misanalyzed extra lines (see above). The corresponding consequences on the correlation analysis of vibronic level spacings are discussed in Sec. V.

3. Comparison with Hiraoka's results

Only 15 of our vibronic band origins can be compared to those found by Hiraoka *et al.*[16] in the 18 199–18 492 cm^{-1} common energy range. There is globally a very good agreement with a mean shift of 0.02 cm^{-1} and a standard deviation of 0.09 cm^{-1}. Nevertheless we have observed 11 vibronic levels not reported by Hiraoka. Moreover, they did not analyze their pairs of very close vibronic bands in terms of extra lines. Consequently, they report two pairs of quasidegenerate vibronic bands shifted by less than 1 cm^{-1}, one group of three quasidegenerate bands and one group of four quasidegenerate bands. We interpret each of these groups of bands in terms of only one band with one or a few extra lines. A discussion about rovibronic couplings inducing extra lines is presented in Sec. IV.

IV. STATISTICAL ANALYSIS OF ROTATIONAL AND SPIN-ROTATION CONSTANTS

A. Rotational spacing distribution

We have mentioned in the previous section that one did not obtain the same result when calculating the $\overline{B'}$ rotational constant from $R_2 - P_2$ differences (i.e., $\overline{B}'_{1,3}$) or from $R_4 - P_4$ differences (i.e., $\overline{B}'_{3,5}$). This point is illustrated in Fig. 3. If the concept of rotational constant, within a given vibronic state, were valid, one should find $\overline{B}'_{3,5} = \overline{B}'_{1,3}$, and correspondingly, points on Fig. 3 should be distributed along the straight line. Obviously, this is not the case. In order to predict the distribution of the rotational constant $\overline{B'}$, we have calculated $\overline{B'}$ for the vibrational levels of the electronic ground state in the 16 500–18 500 cm^{-1} energy range by extrapolation from rovibrational constants given by Lafferty and Sams.[23] The corresponding distribution is displayed on Fig. 4, curve a.

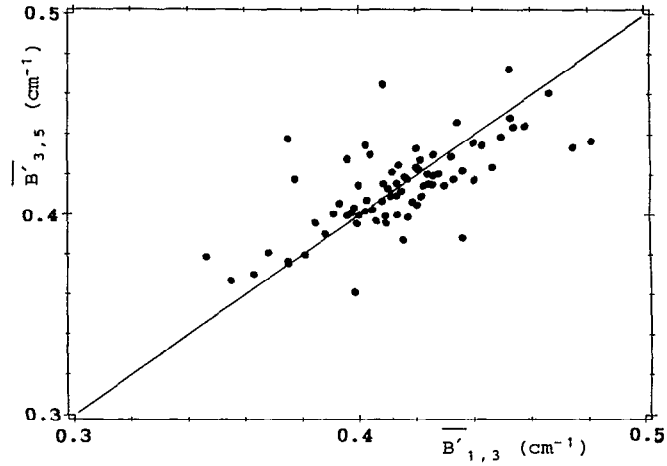

FIG. 3. Correlations between $\overline{B}'_{3,5}$ and $\overline{B}'_{1,3}$ rotational constants. The straight line ($\overline{B}'_{1,3} = \overline{B}'_{3,5}$) corresponds to the rigid rotor model expected in the absence of rovibronic perturbations.

In fact, in this energy range, the real vibronic levels result from interactions between high b_2 (a_1) vibrational levels of the ground state $\tilde{X}\,^2A_1$ with a_1 (b_2) vibrational levels of the excited state $\tilde{A}\,^2B_2$, inducing a very dense visible excitation spectrum. We have calculated 180 b_2 vibrational levels of $\tilde{X}\,^2A_1$ between 16 500 and 18 500 cm^{-1} and about 30 a_1 vibrational levels in $\tilde{A}\,^2B_2$. These 180 b_2 levels have been obtained by extrapolating the 191 observed vibrational levels in the 0–10 000 cm^{-1} energy range of LIDFS (see Delon

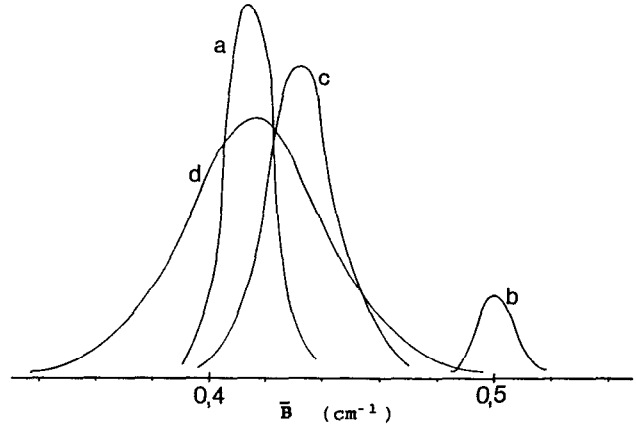

FIG. 4. Distribution of rotational constant $\overline{B'}$ (see the text).

and Jost[15]). These 191 levels have been fitted with a set of 24 Dunham parameters that have been used for the above mentioned extrapolation. The 30 vibronic levels of the $\tilde{A}\,^2B_2$ state correspond to an evaluation based on *ab initio* calculations previously mentioned.[11,12] The expected $\overline{B'}$ constant rotational distribution of $\tilde{A}\,^2B_2$ vibrational levels is concentrated around 0.5 cm^{-1} as displayed in Fig. 4, curve b. The $\overline{B'}$ mean value in the $\tilde{A}\,^2B_2$ state is different from that of the ground state, mainly because the equilibrium angle is 103°, compared to 134° for the ground state (see Refs. 11 or 12). Consequently, if only pure vibronic coupling is assumed, one should obtain the distribution labeled *c* in Fig. 4: each vibronic level has a well-defined $\overline{B'}$ value that is expected to be a weighted average of the different $\overline{B'}$ constants of the involved zeroth-order basis states. In this model of pure vibronic coupling, $\overline{B'}$ still remains a constant, i.e., $\overline{B}'_{1,3} = \overline{B}'_{3,5}$. To explain the inequality of $\overline{B}'_{1,3}$ and $\overline{B}'_{3,5}$ shown in Fig. 3, *ro*vibronic couplings must be taken into account. As explained in Sec. IV B, these *ro*vibronic couplings act on individual J components in a random way, destroying the initial regular rotational spacings of a given vibronic level. Consequently, the distribution *c* on Fig. 4 spreads like distribution *d* and, more strikingly, the $\overline{B}'_{1,3}/\overline{B}'_{3,5}$ ratio is spread out, as displayed on Fig. 3. This explanation implies that N′ is not a very good quantum number anymore. To study this problem thoroughly, we consider the fine structure splitting distribution.

B. Fine structure splitting distribution

For a given vibronic level, we observe that the fine structure constant obtained from $N' = 1$ is not the same as that obtained from $N' = 3$ (see Sec. III) as displayed in Fig. 5. This situation is qualitatively the same as for the $\overline{B'}$ rotational constant. In fact, the *ro*vibronic interactions act selectively on individual J' levels and not globally on N' levels. Let us focus on $N' = 1$, and accordingly on the corresponding fine structure levels $J = 1/2$ and $J = 3/2$. Figure 6 depicts

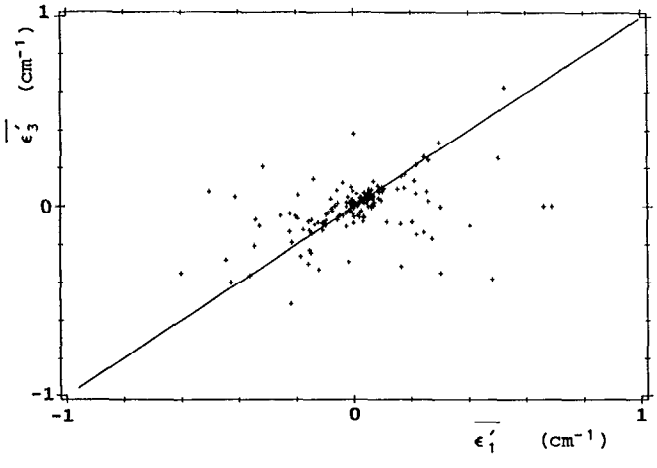

FIG. 5. Correlations between $\overline{\epsilon}'_3$ and $\overline{\epsilon}'_1$ fine structure constants. The straight line ($\overline{\epsilon}'_3 = \overline{\epsilon}'_1$) corresponds to the expected fine structure splittings in the absence of rovibronic perturbations.

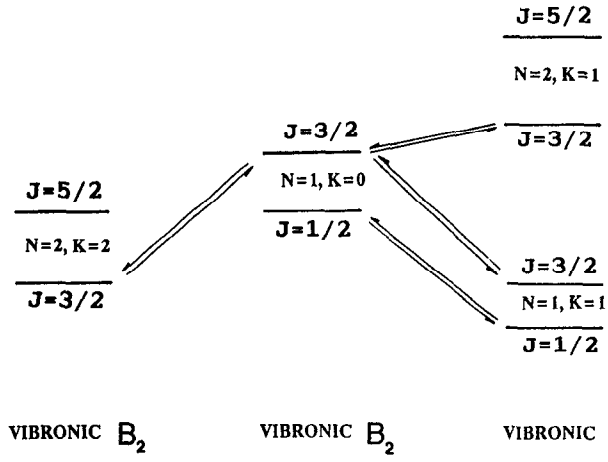

FIG. 6. Possible rovibronic interactions of a $|N = 1, K = 0, J = \mp 1/2\rangle$ level: the total rovibronic symmetry (A_2) is preserved and J is assumed to be a good quantum number.

the different interactions that may create $J' = 1/2$ and/or $J' = 3/2$ extra lines. One ($N = 1, K = 0, J = 1/2$) rotational level of a given B_2 vibronic level can interact only with ($N = 1, K = 1, J = 1/2$) (vibronic A_1) levels while a ($N = 1$, $K = 0, J = 3/2$) level (B_2 vibronic) may interact with ($N = 1, K = 1, J = 3/2$) (A_1 vibronic), ($N = 2, K = 1$, $J = 3/2$) (A_1 vibronic), and ($N = 2, K = 2, J = 3/2$) (B_2 vibronic) levels. Except for the case of mixing with ($N = 2, K = 2, J = 3/2$) levels, the vibronic symmetry of the perturber is A_1, thus implying a breakdown of the vibronic symmetry and of the corresponding fluorescence selection rules. This phenomenon has been observed systematically in LIDFS, observed from highly excited energy levels, located around 23 000 cm^{-1} (see Delon and Jost[15]). On the contrary, after excitation in the "red" part of the excitation spectrum (see Bist and Brand,[24] Brand *et al.*,[25] and Chen *et al.*[26]) the corresponding LIDFS do not contain transitions toward b_2 vibrational levels of the ground state. This means that in the 16 500–18 500 cm^{-1} range, rovibronic interactions remain local, i.e., can be treated as perturbations. At higher energies however, around 23 000 cm^{-1}, the excited B_2 vibronic levels are strongly *ro*vibronically coupled with A_1 vibronic levels. As explained in Sec. III A, when a local rotational perturbation occurs in the red part of the excitation spectrum, we have performed a two state deperturbation based on the observed intensity ratio of the "main" and "extra" lines and on the energy difference of the two observed levels. Of course, *ro*vibronic interactions may occur simultaneously with more than one level. Consequently the calculated $\overline{B}'_{1,3}$ and $\overline{B}'_{3,5}$ are "perturbed" rotational constants. To obtain quantitative information about *ro*vibronic interactions, we have also observed Zeeman spectra (in the 0–8 T range) of seven B_2 vibronic $N = 1$, $K = 0$ levels of about 17 500 cm^{-1} energy.[27] In these spectra the *ro*vibronic interactions, which occur between $M_s = +1/2$ and $M_s = -1/2$ spin sublevels, are observed via anticrossings, allowing us to obtain the corresponding matrix elements and selection rules. We have found that second-order spin–orbit

interaction, usually named spin–rotation, can explain most of the observed interactions. Furthermore, we have been able to follow versus the magnetic field, the energy of two $J = 3/2$ zero field extra lines, and we conclude that these two extra lines are due to an accidental perturbation and do not correspond to an additional vibronic level of B_2 symmetry that has been "missed" in our zero field excitation spectrum. The assignment of the perturber is not yet definitive but the most probable assignment is a $(J = 3/2, N = 1, K = 1)$ level of a vibronic state of A_1 symmetry.

V. VIBRONIC ENERGY CORRELATIONS AND QUANTUM CHAOS

In this section we analyze the correlations between vibronic energy levels of NO_2. We refer to the standard model of Gaussian orthogonal ensemble (GOE)[1,28] which gives the correlation properties of "fully" chaotic systems.

As explained above, the 166 B_2 vibronic levels observed from 16 319–18 502 cm^{-1} are perturbed by rovibronic interactions (mainly due to second-order spin–orbit interactions). However, the corresponding energy shifts are very small, (on average, much less than 1 cm^{-1}) when compared to the mean level spacing of about 12 cm^{-1}. Consequently, we consider that vibronic energies, extrapolated to $N = 0$, $K = 0$ as given in Table II, are very close to the pure vibronic energy levels of NO_2, and these vibronic energies, which result from couplings between electronic and vibrational motions can now be analyzed. As previously reported by Smalley *et al.*,[8] no recognizable vibrational regularity is discernable in the visible excitation spectrum of NO_2 (see below the $|FT|^2$ of the spectrum). In our case, none of the 166 vibronic energy levels between 16 319 and 18 502 cm^{-1} can be assigned electronically [as one of the two electronic states ($\tilde{X}\,^2A_1$ or $\tilde{A}\,^2B_2$)] nor vibrationally, with three vibrational quantum numbers. Each vibronic B_2 (respectively, A_1) eigenstate results from the vibronic coupling of at least one a_1 (respectively, b_2) vibrational level of $\tilde{A}\,^2B_2$ with several high b_2 (respectively, a_1) vibrational levels of the ground state. It is known that, due to vibronic interactions, each zeroth-order vibrational level of $\tilde{A}\,^2B_2$ can imprint its electronic signature into a manifold of high energy vibrational levels of the ground state.[26] This explains the anomalously large number of vibronic bands observed in the visible excitation spectrum (see Haller *et al.*[7,29]). However, it may be possible to assign the dominant "parent" vibrational level of $\tilde{A}\,^2B_2$ character by observation of LIDFS.[25,26] By extrapolating the density of observed vibrational states in $\tilde{X}\,^2A_1$ from 0–10 000 cm^{-1}, one can calculate the average spacing between b_2 levels of $\tilde{X}\,^2A_1$: ~ 11 cm^{-1} in the 16 500–18 500 cm^{-1} energy range. On the other hand, *ab initio* values for $\tilde{A}\,^2B_2$ harmonic frequencies and the assumption that the vibrationless level of $\tilde{A}\,^2B_2$ lies around 9720 cm^{-1} (see Gillispie *et al.*[12] and Delon and Jost[15]), imply that a_1 vibrational levels of $\tilde{A}\,^2B_2$ are on average separated by 80 cm^{-1} in the same 16 500–18 500 cm^{-1} energy range. If one takes into account anharmonicities in the excited state and uses for them the values of the $\tilde{X}\,^2A_1$ state, the mean spacing between a_1 levels of $\tilde{A}\,^2B_2$ is reduced from 80 down to ~ 60 cm^{-1}. Strong vibronic couplings (nonadiabatic effects) mix these two sets of levels together in such a way that no regularity can be observed in the spectrum above $\sim 16\,500$ cm^{-1}. On the contrary, the low resolution absorption spectra from Gillispie and Khan[30] display, from 9000–6000 Å, a strong intensity modulation that corresponds to the bending frequency in $\tilde{A}\,^2B_2$, of about 720 cm^{-1}. This observation means that vibronic interactions do not set in abruptly above the conical intersection. In this intermediate energy range (i.e., roughly from $\sim 10\,000$ to 16 000 cm^{-1}), vibronic interactions already couple each $\tilde{A}\,^2B_2$ "parent" level to some $\tilde{X}\,^2A_1$ "daughter" levels but do not yet wash out the bending progression in the excitation spectrum. One implication of strong mixing (required for complete quantum chaos) is that such regularities have disappeared.

The analysis of short range correlations (Sec. V B) and long range correlations (Sec. V C) require the knowledge of the secular behavior of the integrated density of states discussed in Sec. V A.

We have not presented here a statistical analysis of the band intensities given in Tables I or II because we do not have a good knowledge of the energy dependence of the measured intensities (see Sec. V A). However, the observed intensity distribution is not far from the Porter–Thomas law [i.e., the expected distribution for the GOE model (see Ref. 1)], if we take into account the missing levels that all have a weak intensity.

A. Secular behavior of the integrated density of states and unfolding procedure

1. Fit of the integrated density of states

We now present the method for analyzing the correlations. It is important to know that only density fluctuations are relevant to the study of correlation properties. Therefore, the integrated density of levels $N(E)$ (that is, the staircase function giving the number of energy levels below an energy E) should be separated into a smooth part $N_{av}(E)$ and the remainder, which defines the fluctuating part $N_{fl}(E)$ of $N(E)$ (see Ref. 1);

$$N(E) = N_{av}(E) + N_{fl}(E). \tag{2}$$

When the potential energy surface (PES) is known, one can calculate $N_{av}(E)$ following simple semiclassical rules.[31] Unfortunately in most real cases, one does not know the PES. In the case of a nonlinear $N =$ atom molecule (i.e., $n = 3N - 6$ vibrational degrees of freedom), it is known from semiclassical and harmonic approximations (Marcus and Rice[32]) that

$$N_{av}(E) = \frac{(E + E^0)^n}{n! \prod_{i=1}^{n} (\omega_i)}, \tag{3}$$

where E is the vibrational energy in excess of the zero point energy E^0 and ω_i are the harmonic frequencies. This formula gives the dominant contribution: $N_{av}(E) \propto E^n$. In the case of NO_2, $N_{av}(E) \sim E^3$. In fact, anharmonicities are such that

the effective density of states increases slightly faster than E^3. We have calculated numerically the integrated density of vibronic levels with the Dunham polynomial expansion given either by Lafferty and Sams[23] or by Delon and Jost.[15] This integrated density was then fitted with polynomial expansions in energy, all starting with a cubic term. As a result, the two-term limited power expansion

$$N_{av}(E) = a_3E^3 + a_6E^6 \quad (4)$$

appears very satisfactory. Figure 7 displays the $N(E)$ of our set of 166 observed levels in the 16 319–18 502 cm^{-1} range and the corresponding fit with the above formula.[1] It appears that the slope discontinuity at 16 500 cm^{-1} clearly indicates missing vibronic levels below this energy. Consequently, we will hereafter restrict our level-spacing statistical analysis to the 16 500–18 500 cm^{-1} energy range, which contains 159 observed levels.

2. Comparison between the observed and predicted number of states

It would be of interest to compare the 159 observed levels with the corresponding expected number of levels. To this end we have observed laser induced dispersed fluorescence spectra from 11 high vibronic levels around 23 000 cm^{-1} (Delon and Jost[15]). The complete set of 191 observed $\tilde{X}\,^2A_1$ vibrational levels below 10 000 cm^{-1} are well fitted with a 24 parameter Dunham expansion. The extrapolation of this Dunham expansion to the 16 500–18 502 cm^{-1} range, produces 180 b_2 vibrational levels of $\tilde{X}\,^2A_1$. Note once again it is the mixing between this dense manifold of $\tilde{X}\,^2A_1$ vibrational levels with those of the $\tilde{A}\,^2B_2$ state that explains the dense NO_2 excitation spectra in the visible. The total number of mixed (and thus observable) levels of B_2 vibronic symmetry, taking into account the 30 levels of the $\tilde{A}\,^2B_2$ state in the same energy range, is thus about 210 in the 16 500–18 502 cm^{-1} energy range. This should be compared with the 159 observed levels in the corresponding range. In comparison, 17 levels are predicted from 16 319–16 500 cm^{-1} while only seven have been observed. This last point confirms (see Fig. 7) that more levels are missing below 16 500 cm^{-1} in our excitation spectrum as well as that in Smalley *et al.*[8] and Persch *et al.*[9] To conclude, in the 16 500–18 502 cm^{-1} energy range, about 75% of all B_2 vibronic levels have been observed. Missing levels are due either to the unfavorable Franck–Condon factor with the initial ground state, or to the fact that some b_2 levels of $\tilde{X}\,^2A_1$ are not mixed well enough with the a_1 level manifold of $\tilde{A}\,^2B_2$. However, our percentage of missing levels is significantly smaller than that obtained by Persch *et al.*[9] Zimmermann *et al.*[22] have performed a statistical analysis on a set of 141 observed levels in the 14 880–17 521 cm^{-1} energy range, where our model predicts 222 levels. Note that the harmonic model of Zimmermann *et al.*[29] predicts 175 levels in this energy range and that anharmonicities should increase this number. Moreover, 25 of these 141 levels are spurious, most of them being hot bands (see Sec. III B). As a result we estimate that the 141 level set of Persch *et al.* contains only 116 "true" levels and 25 spurious ones, and that these 116 "true" levels represent 52% (or 116/222) of the total number of levels predicted in this energy range. Obviously, the NO_2 excitation (or absorption) spectrum being globally weaker when going to the red (see Fig. 3 of Ref. 30), more missing levels are expected in the 14 880–17 521 cm^{-1} energy range than in our 16 500–18 502 cm^{-1} range with the same detection efficiency. In other words, it is easier to study the yellow and green parts of the NO_2 spectrum, at least when the goal is the completeness of the vibronic spectrum. The above 52% estimation does not agree with that of Zimmermann *et al.*,[22] who found only 8% missing levels by comparing the intensity distribution of their 141 bands with the Porter–Thomas distribution. Their comparison is biased for two reasons. First, their set of 141 bands includes 22 hot bands, as explained in Secs. III A and III B. These hot bands being statistically 75 times weaker compared with the cold ones, the intensity distribution is significantly affected. Second, the global intensity evolution of the excitation spectrum displayed in Fig. 2 of Ref. 7 should be taken into account before any comparison with the Porter–Thomas law is made. For these two reasons the intensity distribution given in Fig. 1 by Zimmermann *et al.*[22] should be reanalyzed.

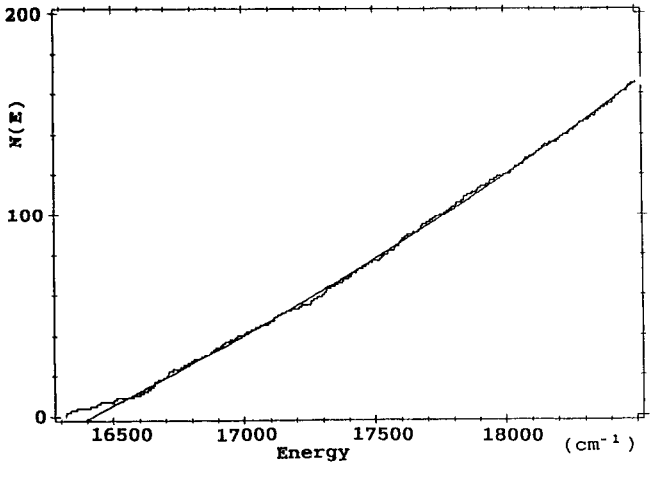

FIG. 7. Integrated density of states $N(E)$. The experimental staircase curve clearly displays missing levels below 16 500 cm^{-1}. $N(E)$ is well fitted with the polynomial expansion: $N_{av}(E) = N_0 + a_3E^3 + a_6E^6(-N_0$ is a rough estimate of the absolute energy rank number of the first level of our sequence).

3. The unfolding procedure

We have shown that the smooth part of the integrated density of states, $N_{av}(E)$, can be well fitted with a two-term limited polynomial expansion, like formula (4). Following Brody *et al.*,[1] the unfolded spectrum $\{x_i\}$ is then obtained with the transformation

$$E_i \rightarrow x_i = N_{av}(E_i). \quad (5)$$

We prefer unfolding the spectra with a smooth polynomial expansion like formula (4) rather than performing cubic spline interpolation, as performed by Zimmermann *et al.*[22] We have observed that a cubic spline unfolding reduces the fluctuations $N_{fl}(E)$ by an amount that depends on the

mean distance between the cubic spline constraint points. In Appendix C we show that the unfolding procedure has large consequences on long range correlations, the short range correlations being much less sensitive to the unfolding procedure.

B. Short range correlations within energy level spacings

In this section we present the statistical analysis of the energy level spacings between consecutive levels: the NND. Regular systems, i.e., systems whose Hamiltonian is integrable, are generically characterized by a Poisson distribution, $P(S) = \exp(-S)$; S being the normalized spacings. The Poisson distribution peaks at the origin, $S = 0$. This means physically that accidental degeneracies may occur. On the contrary, when the system is fully chaotic, one observes level repulsion. A very good approximation for the NND of the GOE is the Wigner distribution (Ref. 1):

$$P(S) = (\pi/2)Se^{-(\pi/4)S^2}. \tag{6}$$

Figure 8 displays the NND histogram for our unfolded set of 159 observed vibronic levels from 16 500–18 502 cm^{-1}. Our results are in reasonable agreement with the Wigner law. Quantitatively, the Wigner law predicts σ, the square root of the second moment $[\overline{(S-\bar{S})^2}]^{1/2}$, to be 0.52, while we find $\sigma = 0.61$.

This deviation may be due to missing levels. We conclude that the observed NND is in agreement with the prediction of the GOE model. However, the NND is only a robust (i.e., weakly dependent on the unfolding procedure) test of short range correlations, but it does not contain a lot of physical information, especially about the time evolution of the system. By contrast, the long range correlations contain more physical information but are much more sensitive to the unfolding procedure, as explained below.

C. Long range correlations within energy level spacings

Long range correlations between energy levels contain most of the significant information on the dynamics of the corresponding physical system. We consider here three standard methods for analyzing these long range correlations: $\Sigma^2(L)$, $\Delta_3(L)$ (see Ref. 1) and $\overline{|FT|^2}$ (smoothed Fourier transform) (see Ref. 2 and Appendix L of Ref. 1). The key point is that these three methods are nothing more than three kinds of smoothing procedure for the $|FT|^2$ of the stick spectrum. This $|FT|^2$ is related to the two-level form factor $b_2(t)$, that is, the Fourier transform of the two level cluster function $Y_2(\Delta E)$ of Dyson and Mehta.[28]

The general relations between the $|FT|^2$ and the correlations are detailed in Appendix A. The analytic relations between $|FT|^2$, $\Sigma^2(L)$, and $\Delta_3(L)$ are given in Appendix B. Here L is a dimensionless energy expressed in units of the average level spacing.

As we have pointed out in Sec. V A, the initial spectrum (stick spectrum) should be unfolded and any unfolding method reduces the long range correlations. The relevant problem is only to determine the maximum value for L (or correspondingly the minimum value for t) for which the correlations remain meaningful, i.e., not biased by the unfolding procedure. This point is discussed in Appendix C. We present below the long range correlations of our set of 159 vibronic levels of NO_2, first with $\Sigma^2(L)$ and then with the $|FT|^2$ method.

1. $\Sigma^2(L)$ analysis

Figure 9 shows $\Sigma^2(L)$ for our observed set of 159 vibronic levels which appears to be close to the GOE prediction [displayed on curve (a)] for chaotic systems: these are characterized by the existence of long range correlations (spectral rigidity or stiffness). The GOE model gives

$$\Sigma^2(L) = (2/\pi^2)\ln(L) + 0.44 + O(1/L\pi^2). \tag{7}$$

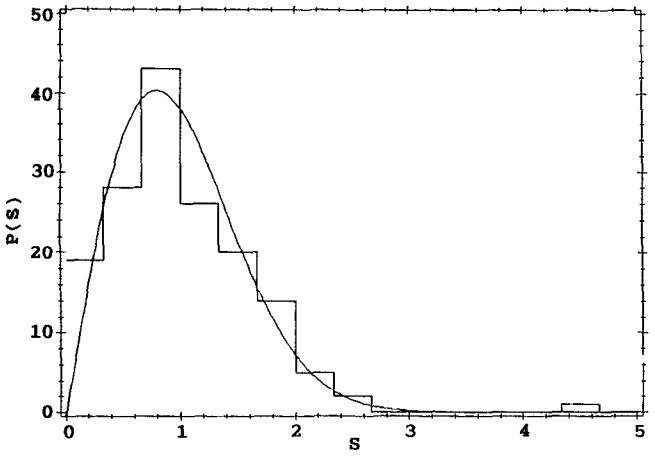

FIG. 8. Nearest neighbor distribution $P(S)$ for the set of 159 vibronic energy levels from 16 500 to 18 502 cm^{-1}. The experimental histogram is in agreement with the Wigner law (smooth curve) for fully chaotic systems.

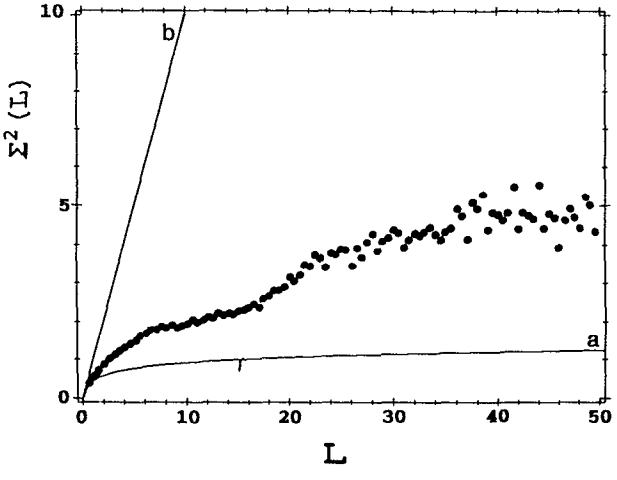

FIG. 9. $\Sigma^2(L)$ statistics performed on the same set of vibronic energy levels as for $P(S)$. (a) The GOE prediction for fully chaotic systems. (b) The prediction for a spectrum without any level correlations.

Regular systems are generically characterized by Poisson statistics, namely $\Sigma^2(L) = L$ [see (b) of Fig. 9]. However, significant deviations from the Poisson law can be observed for triatomic molecules in the regular regime as discussed recently by Hamilton.[33] This deviation is particularly important when there are near resonance conditions in the harmonic frequencies. For example, below 10 000 cm^{-1}, the NO_2 vibrational spectrum is regular,[15] but does not follow precisely Poisson statistics because $2\omega_2 \simeq \omega_1 \simeq \omega_3$. However, the levels calculated with the above mentioned Dunham expansion[15] in the 16 500–18 502 cm^{-1} energy range follow Poisson statistics because the anharmonicities have destroyed the approximate vibrational frequency resonances. Last but not least we have numerically checked that the deviation of our $\Sigma^2(L)$ from the GOE can be explained solely by the 25% missing levels, if one assumes that these levels are randomly distributed.

Now, we would like to compare our results on $\Sigma^2(L)$ to those of Zimmermann *et al.*[22,9] on $\Delta_3(L)$. We first emphasize that unfolding procedures reduce the long range correlations, as explained in Appendix C. Second, it is first important to note that $\Delta_3(L)$ and $\Sigma^2(L)$ do not measure fluctuations on the same range of L. This point is discussed in Appendix B. We have analyzed correlations within the set of 141 vibronic energy levels of Persch *et al.*[9] The corresponding $N(E)$ and $N_{av}(E)$ [according to Eq. (4)] are displayed in Fig. 10 and the $\Sigma^2(L)$ statistic is shown in Fig. 11. As a result, we find much smaller long range correlation than we do with our set of 159 vibronic levels. This is mainly due to the existence of 25 spurious levels and to about 50% missing levels in their data. A more general method for studying correlations is the statistical Fourier transform analysis presented in the following section.

2. Fourier transform analysis

The Fourier transform of a spectrum contains information on line positions, linewidths, and amplitudes. When the correlations between line positions (or energy levels) are studied, it is better to construct a stick spectrum of equal amplitude and then to study these correlations. However, when the experimental spectrum is not well resolved, the extraction of a stick spectrum is ambiguous and therefore the direct FT of the experimental spectrum is a well adapted method to obtain the corresponding correlations, with the drawback due to intensity and width distribution discussed in Ref. 2. Our NO_2 vibronic spectrum is well resolved and can be analyzed in terms of a stick spectrum.

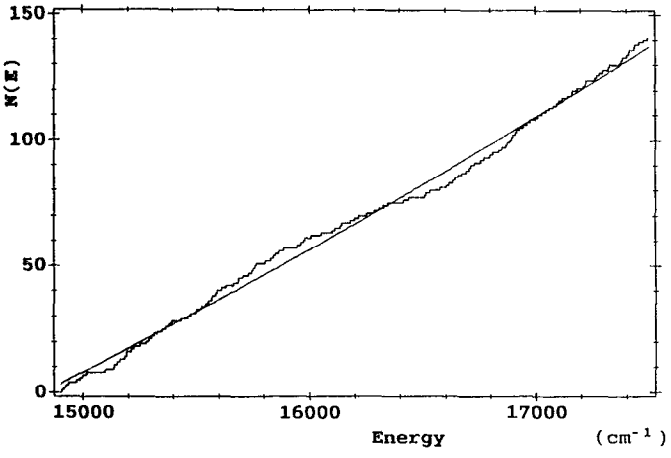

FIG. 10. Integrated density of states $N(E)$ from the 141 vibronic band origins of Persch *et al.* (Ref. 9). The experimental staircase curve oscillates with a large very low frequency component around the polynomial expansion fit: $N_{av}(E) = N_0 + a_3E^3 + a_6E^6$.

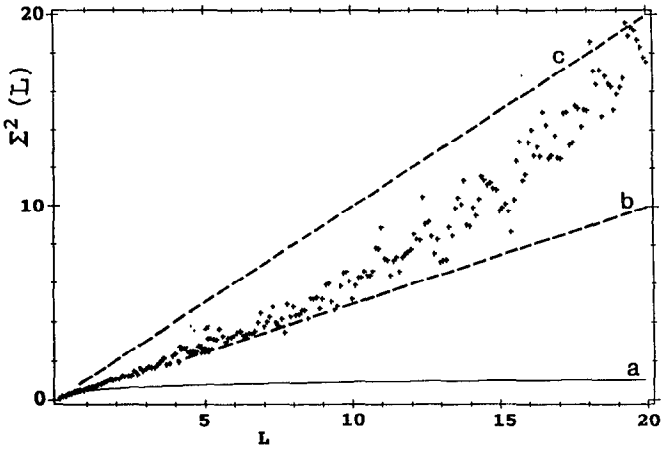

FIG. 11. $\Sigma^2(L)$ statistics performed on the 141 vibronic levels of Persch *et al.*, unfolded with the polynomial expansion shown in Fig. 10. (a) The GOE prediction. (b) The statistics of a fictitious system that would have the same NND as the Persch *et al.* set of vibronic levels but no long range correlations. (c) The statistics of a Poisson distribution.

The meaning of the $|FT|^2$ of a stick spectrum in terms of correlations is given in Appendix A. It is necessary to distinguish between the $|FT|^2$ of the original stick spectrum (i.e., before unfolding), which may reveal the existence of periodic (or regular) motion(s) (if any), and the $|FT|^2$ of the unfolded stick spectrum, which contains $[1 - b_2(t)]$.

In the case of our NO_2 spectrum no regular motion has been observed, and, consequently, we discuss only $|FT|^2$ of the unfolded spectrum, which is displayed in Fig. 12.

Now three related questions arise. (i) How to smooth the $|FT|^2$ in order to best display the correlations, or, more specifically, $[1 - b_2(t)]$; (ii) how the $|FT|^2$ is related to the other correlations measurements, $\Sigma^2(L)$ and $\Delta_3(L)$; and (iii) which unfolding procedure is legitimate?

These questions are treated in Appendices A, B, and C, respectively.

Since globally our $\Sigma^2(L)$ (Fig. 9) and our $|FT|^2$ (Fig. 12) display strong long range correlations, we can now discuss the behavior and the validity of these correlations for large L, or equivalently, for short time.

In any case, the number of relevant pieces of information for large L (or small t) is very small: In the $|FT|^2$, the number of points to smooth over for small t is very small, due to the discrete nature of the fast Fourier transform algorithm. This is a consequence of the uncertainty principle, which governs the recovery of low frequency Fourier components from a signal of finite duration.

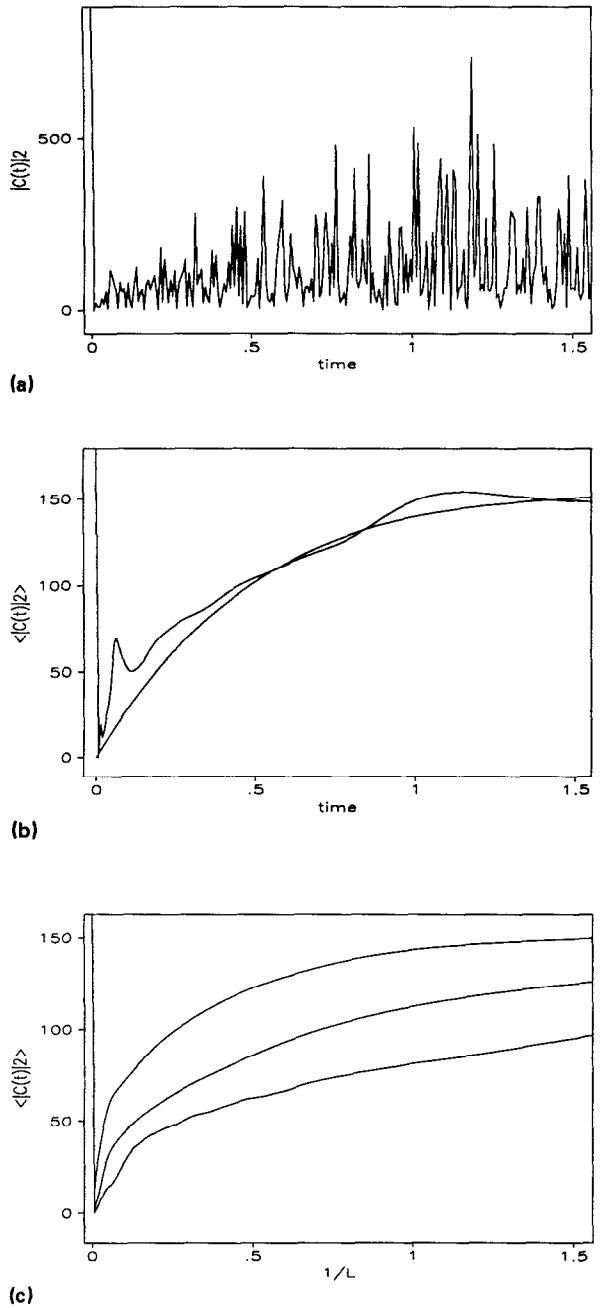

FIG. 12. $|FT|^2$ of our data (16 500–18 500 cm^{-1}), unfolded with $N(E) = N_0 + a_3E^3 + a_6E^6$. (a) Unsmoothed: one channel is equal to $t = 1/N$, where N is the number of levels in the spectrum. (b) Smoothed with a Gaussian kernel $K(L,t) = (1/\sigma\sqrt{2\pi})\exp[-(t-1/L)^2/2\sigma^2]$ of center $1/L$ and root mean square width $\sigma = 1/5L$, and compared with the $\langle|C(t)|^2\rangle$ GOE prediction smoothed with the same kernel. The experimental $|C(t)|^2$ being less smoothed at short times, results in the two residual peaks. However, for times shorter than 0.5 (in units of level density) the experimental curve is located above the GOE prediction, after which it oscillates around its asymptotic behavior line. (c) Smoothed with Δ_3 (top), half-Gaussian beginning at $t = 0$ with $\sigma = 1/L$ (middle), Σ^2 (bottom). Beware that in all cases the abcissa is $1/L \propto$ time (reduced unit) and the kernels have been normalized to unit area between $t = 0^+$ and $t = +\infty$ (instead of L and $L/15$ between $-\infty$ and $+\infty$ for the usual Σ^2 and Δ_3 kernels). Notice that the three curves in (c) seem to differ vertically while they actually differ horizontally, because the meaning of the parameter L is different in the three cases. The fact that $\Delta_3(L)$ is roughly equivalent to $\Sigma^2(L/4)$ or to Gauss $(L/2)$ is seen from the ratio of the slopes of the three curves at $t = 0$ (see Appendix B). All curves in (a), (b), and (c) have the same asymptote at $t = +\infty$, that is $N = 159$, the number of levels.

Equivalently, the uncertainties in $\Sigma^2(L)$ [or $\Delta_3(L)$] increase with L and the meaning of $\Sigma^2(L)$ for large L should be discussed.

In order to study the upper limit of L, for which long range correlations exist and are meaningful, we think that it is better to look first at the unsmoothed $|FT|^2$ of the spectrum [Fig. 12(a)], keeping in mind the statistical properties and the physical meaning of the "speckle noise" discussed in Appendix A.

Concerning the unfolding, any procedure reduces $[1 - b_2(t)]$, i.e., introduces spurious correlations, especially for small t (i.e., for large L). The relevant problem is only to determine the range of t, from 0^+ to t_{max}, for which the chosen unfolding procedure has reduced significantly the $[1 - b_2(t)]$ function. Conversely, the range, $t > t_{max}$ is not affected by the unfolding procedure. We have numerically observed that our unfolding procedure (see Sec. V A) reduces $[1 - b_2(t)]$ only for the first two channels of the $|FT|^2$, i.e., for $t \lesssim 1/80$ or equivalently $L \gtrsim 80$ (see FFT in Appendix A).

We conclude that our NO_2 vibronic spectrum is correlated up to at least $L = 50$ or, equivalently, on an energy range of the order of 670 cm^{-1}.

Obviously, the real correlation length of the NO_2 vibronic levels may be larger but our finite set of vibronic levels does not allow us to observe correlations beyond $L = 50$, i.e., beyond 50 average level spacings.

Our results do not contradict those of Zimmermann *et al.*,[22,9] but instead they complement and improve their results.

First we should remark that the energy ranges of the two sets of vibronic levels overlap but do not coincide, and that the corresponding correlations may be different. Second, the correlations put into evidence by Zimmermann *et al.*[22,9] with $\Delta_3(L)$ ranging up to $L = 15$ are equivalent to those evidenced with $\Sigma^2(L)$ ranging up to $L = 4$ (Fig. 11). The reason for this reduced range of L is explained in Appendix B. Over this reduced range of L we conclude that the correlations measured with $\Sigma^2(L)$ in the data of Persch *et al.*[9] (Fig. 11) are in agreement with those measured with $\Sigma^2(L)$ in our data (Fig. 9). In addition to this, the necessity to unfold the Persch *et al.*[9] spectrum with a very flexible function (cubic spline with five adjustable knots) precludes study of their vibronic set correlations over a larger range of L. This situation arises because there are many missing and spurious levels in Persch's spectrum (see Sec. V A), which induce low frequency components in $N(E)$, as explained in Appendix C.

In summary, our better set of vibronic levels, more complete and with fewer spurious levels, allows us to document long range correlations up to at least $L = 50$. A longer sequence of vibronic levels is necessary to extend the analysis of long range correlations to higher values of L.

We plan to extend to higher energies the set of vibronic levels of NO_2 in order to increase the upper limit for the correlation length.

A significant extension of the vibronic set to lower energies seems difficult because the corresponding band intensities decrease globally and, consequently, the percentage of

missing levels increases. This phenomenon can be observed in both Figs. 7 and 11 below 16 500 cm^{-1}.

This is consistent with the NO_2 absorption spectrum of Gillispie and Khan,[30] which shows a minimum of absorption around 16 200 cm^{-1}, leading obviously to a larger fraction of missing levels.

VI. CONCLUSIONS

Among our set of 166 observed vibronic levels (or cold bands), more than 45 have not been previously observed and/or identified. Moreover we have interpreted the irregular rotational fine structure spacings that have caused spurious vibronic levels to be introduced in previous works. By comparison to the observed and calculated vibronic density of states, we find only 25% levels missing from our set. The correlation analysis of vibronic energy spacings shows a good agreement with the GOE model prediction if we take into account the above mentioned missing levels. This result confirms that the conical intersection of the PES of the $\tilde{X}\,^2A_1$ and $\tilde{A}\,^2B_2$ states induces vibronic chaos, as predicted by Zimmermann *et al.*[29] This vibronic interaction can be studied experimentally by observing the set of vibronic levels in the 10 000–16 000 cm^{-1} energy range in which chaos should appear progressively, the region around or just above 10 000 cm^{-1} being the most interesting. Unfortunately the levels in this energy region are difficult to observe (see, for example, Figs. 3 and 4 of Gillispie and Khan[30]). We are now trying to observe these levels with three techniques: (i) excitation spectrum using a Ti:sapphire laser, (ii) intracavity laser absorption spectrum (ICLAS) using a supersonic jet, and (iii) laser induced dispersed fluorescence spectrum (LIDFS) (see Ref. 15).

APPENDIX A: CORRELATIONS MEASUREMENT BY $|FT|^2$

The basic statistical quantity that characterizes a spectrum is Dyson's two-level cluster function $Y_2(\Delta E)$ or its Fourier transform, the two-level form factor $b_2(t)$ (see Refs. 1, 28, and 34).

The key point in correlation measurement by $|FT|^2$ is that the two-level form factor $b_2(t)$ can be recovered from the square of the modulus of the Fourier transform of the spectrum. In the case of a stick spectrum whose sticks all have the same intensity:

$$S(E) = \sum_i \delta(E - E_i); \tag{A1}$$

then

$$|C(t)|^2 = \sum_{i,j} e^{2i\pi(E_i - E_j)t}. \tag{A2}$$

Replacing the discrete sum over levels by an average over their probability distribution results in

$$\langle |C(t)|^2 \rangle = \left| \int R_1(E) e^{2i\pi Et}\, dE \right|^2 + \int R_1(E)\, dE - \int\int T_2(E,E') e^{2i\pi(E-E')t}\, dE\, dE', \tag{A3}$$

where $R_1(E)$ is the level density and $T_2(E,E')$ is the two-level correlation function, as defined by Mehta.[28] If the spectrum is unfolded $R_1(E) = 1$, and $T_2(E,E') = Y_2(E - E')$. Here E is a reduced energy expressed in units of mean level spacing $\overline{\Delta E}$ and t is a time expressed in units of level density $\rho = 1/\overline{\Delta E}$. Then Eq. (11) reduces term by term to

$$\langle |C(t)|^2 \rangle = N^2 (\sin \pi Nt / \pi Nt)^2 + N - Nb_2(t), \tag{A4}$$

where N is the number of levels in the spectrum.

$\langle |C(t)|^2 \rangle$ contains two components: (i) a "fast component" [first term in (A4)] due to the finite length of the spectrum whose contribution is N^2 at $t = 0$ (N being the total number of levels); (ii) A "slow component" [the second and third terms in (A4)] of amplitude proportional to N, which contains the information we look for in level spacing correlations.

For intermediate times (roughly from $t = 0^+$ to $t \approx 1$) one gets $\langle |C(t)|^2 \rangle = N[1 - b_2(t)]$. In the case of a Poisson spectrum $Y_2(\Delta E) = 0$ and then $\langle |C(t)|^2 \rangle = N$ for $t > 0$. On the contrary, fully chaotic systems following GOE statistics correspond to $1 - b_2(t) \simeq 2t$ for $0 < t \lesssim 1$. This is called a correlation hole (see Fig. 12 and Refs. 2 and 35) and means that, due to chaos, the system loses the memory of its initial state as soon as t is greater than 0. For cases intermediate between fully chaotic and regular systems, the correlation hole is less deep and/or abrupt, meaning that for short times the memory is lost progressively. The time at which memory is lost ($t = 0^+$ for fully chaotic systems and $t = +\infty$ for regular systems) can be expressed in terms of energy, which, in turn, can be expressed in units of mean spacing, i.e., in terms of L. In Sec. V, we give a lower limit for L of the order of 50 for the vibronic levels of NO_2.

Note that Berry[36] has shown that, at the semiclassical limit, $\langle |C(t)|^2 \rangle$, or equivalently $1 - b_2(t)$, results from an average over peaks corresponding to closed periodic orbits. The relationship between level statistics and time behavior does not depend on the validity of the semiclassical approximation. This is fortunate in the present experiments where this approximation is not valid, both because of the moderate number ($\approx$4–5) of quanta per mode, and because there is no well-defined semiclassical limit for the interaction between the two different electronic states, $^2A_1$ and $^2B_2$, which dominates the dynamics in NO_2: at the semiclassical limit, the spacing between electronic states must also tend to zero.

Before going any further it is essential to notice that the derivation of Eq. (A3) is obtained by replacing a discrete sum over the levels of the spectrum by an average over a probability distribution of levels. This corresponds, strictly speaking, to an averaging over an ensemble of spectra (denoted by $\langle \cdots \rangle$ in these equations). In the actual case of a single spectrum, one thinks of statistical properties of level spacings of this spectrum. However, this is different from what has been assumed in the derivation and is also a somewhat ill-defined notion for a finite sample, and this has important consequences. The most evident, when performing the Fourier transform of a single spectrum, is that one does not obtain the smooth curve described by Eqs. (A3) and (A4), but a very "noisy" curve, 100% modulated by spikes, whose correlation times are equal to h times the reciprocal of

the total energy length of the spectrum. The physical origin of this "noise" is that $|C(t)|^2$ contains enough information to reconstruct the very complex original spectrum, within a factor of 2 contained in the discarded phases. This noise is dubbed "speckle noise" in Ref. 2 because it is a property of Fourier transforms analogous to what gives rise to the laser speckle phenomenon. $|C(t)|^2$ is in some sense a much more detailed and less smooth information than the two-level form factor $b_2(t)$. To recover statistical information like $b_2(t)$ from a given sample, it is always necessary to perform some averaging. The finiteness of the sample limits the accuracy of this recovery. The physical meaning of the 100% speckle noise is as follows. The standard error on the measurement of $b_2(t)$ for a given value of t is equal to its average value (not to the square root of the average as in an ordinary Poisson process), and this is independent of the level spacing statistics in the original spectrum. This precludes any accuracy in the measurement for a sharp value of t. These statistical properties of the speckle noise (standard error and time correlation length) are such that it is only possible to recover an average value of $b_2(t)$ over a range δt (in reduced units), with a relative accuracy equal to $1/\sqrt{2N\,\delta t}$. With a given finite sample, it is thus always necessary to compromise between the length of Δt and the accuracy of the averaging over Δt.

Figure 12 of Sec. V displays several examples of smoothing. We emphasize the different aspects of these various smoothed curves, which are discussed in Appendix B.

In this context $\Sigma^2(L)$ and $\Delta_3(L)$ are two standard ways of averaging $1 - b_2(t)$, which are compared in Appendix B.

APPENDIX B: RELATIONS BETWEEN $|FT|^2$, $\Sigma^2(L)$, AND $\Delta_3(L)$

Here $\Sigma^2(L)$ is a smoothed form of the two-level form factor $b_2(t)$, the Fourier transform of Mehta's[28] two-level cluster function $Y_2(\Delta E)$:

$$\Sigma^2(L) = \int_{-\infty}^{+\infty} [1 - b_2(t)]K_\Sigma(L,t)dt, \qquad \text{(B1)}$$

with a weighting function (see Ref. 1):

$$K_\Sigma(L,t) = L^2[\sin(\pi Lt)/\pi Lt]^2, \qquad \text{(B2)}$$

sketched in Fig. 13. $\Sigma^2(L)$ is thus basically a weighting of $1 - b_2(t)$ between 0 and roughly $1/2L$.

Following Brody *et al.*,[1] $\Delta_3(L)$ can be considered as a smoothed value of $\Sigma^2(L)$ between 0 and L:

$$\Delta_3(L) = \frac{2}{L^4}\int_0^L \Sigma^2(s)(L^3 - 2L^2 s + s^3)ds. \qquad \text{(B3)}$$

The corresponding smoothing function is shown in Fig. 14. It thus appears that $\Delta_3(L)$ is an averaging of $\Sigma^2(L)$ between 0 and L with a large weight for small L. Roughly, this means that $\Delta_3(L)$ corresponds to $\Sigma^2(L/4)$ and not to $\Sigma^2(L)$! This can be seen in our data on Fig. 12(c), where the abscissa of the curve corresponding to $\Sigma^2(L)$ should be divided by about 4 for this curve to superimpose approximately onto the curve corresponding to $\Delta_3(L)$.

$\Delta_3(L)$ is thus a smoothing of $[1 - b_2(t)]$ with a weighting function

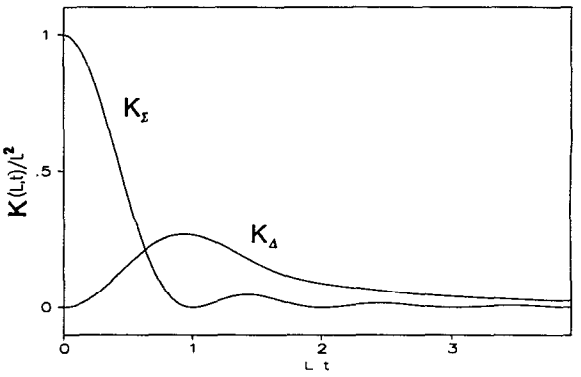

FIG. 13. Weight functions $K(L,t)$ for Σ^2 and Δ_3 smoothing. Note that Σ^2 smoothes approximately between 0 and $1/2L$ at half-height, i.e., around $1/4L$, whereas Δ_3 smoothes between $1/2L$ and $2/L$ (half-height), i.e., around $1/L$. The ratio of smoothing centers is thus 4, so that $\Delta_3(L)$ is roughly equivalent to $\Sigma^2(L/4)$. The Δ_3 kernel is normalized so that its area from $t = -\infty$ to $t = +\infty$ is L as for the Σ^2 kernel (instead of $L/15$ for the usual Δ_3 kernel).

$$K_\Delta(L,t) = L^2[1 - F(y)^2 - 3F'(y)^2]/(2y)^2, \qquad \text{(B4)}$$

with

$$F(y) = \sin y/y \quad \text{and} \quad y = \pi Lt,$$

obtained by combining Eqs. (B1) and (B3) and inverting the order of the integrations.[37] This smoothing function is sketched in Fig. 13 on the same scale in order to illustrate the difference of meaning between $\Sigma^2(L)$ and $\Delta_3(L)$ for the same value of L.

For Poisson statistics $1 - b_2(t) = 1$ for $t > 0$. For GOE statistics, $1 - b_2(t)$ grows linearly from 0^+ and saturates at 1 for $t \approx 1$ in reduced units (i.e., taking an energy unit equal to the mean spacing between levels in the spectrum). Therefore $\Sigma^2(L) = L$ for Poisson statistics because the area of $K_\Sigma(L,t)$ is equal to L, and is proportional to $\mathrm{Log}(L)$ if $1 - b_2(t)$ is proportional to t between 0^+ and $1/L$. Similar conclusions apply to $\Delta_3(L)$, except for the area of $K_\Delta(L,t)$ being equal to $L/15$.

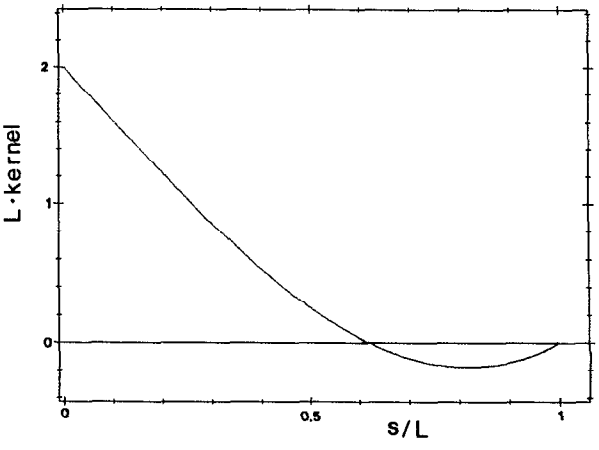

FIG. 14. Kernel relating $\Delta_3(L)$ to $\Sigma^2(L)$ as a smoothing of $\Sigma^2(s)$ between $s = 0$ and $s = L$. It thus appears that $\Delta_3(L)$ is roughly equivalent to an average of Σ^2 around $L/4$.

APPENDIX C: SPURIOUS EFFECTS OF UNFOLDING ON LONG RANGE CORRELATION MEASUREMENTS

First, it is important to understand the problems of unfolding in this context, to note that the first term in Eq. (A4) for an unfolded spectrum, which is by far the largest due to its N^2 coefficient, is exactly zero for each channel except the zeroth, when one uses as usual a discrete Fourier transform algorithm like the FFT. However, when the spectrum has not been correctly unfolded, the corresponding first term in Eq. (A3) is the Fourier transform of the average (nonconstant) density of states $R_1(E)$ and gives an important signal at short times, i.e., at large spectral lengths, on the order of the total energy width of the spectrum.

To interpret the effects of unfolding, it is eventually useful to note that since $N(E)$ is an integral over the spectrum $S(E)$, its Fourier components are those of $S(E)$ divided by t: this will enable us to work and think directly with Figs. 7 and 10 in Sec. V.

We will discuss the problems associated with unfolding on the results of Persch *et al.*,[9] because they are particularly important in this case, which makes them easier to understand. What is immediately seen in Fig. 10 is that the difference between $N(E)$ and $N_{av}(E)$ contains a large very low frequency component of approximately 1500 cm^{-1} period, versus 2500 cm^{-1} for the total range. This low frequency component (contained mainly in channel two in the FFT of the spectrum displayed in Fig. 15(a), when integrated with $K_\Sigma(L,t)$ of Eq. (B2), gives the large quadratic growth of $\Sigma^2(L)$ seen on Fig. 11. When the spectrum is unfolded with a more flexible spline function as was done by Zimmermann *et al.*,[22,9] $N_{av}(E)$ follows this large second channel component, eliminating it from the resulting unfolded spectrum, as seen in Fig. 15(b). This is the reason why the corresponding growth disappears in $\Sigma^2(L)$, leading to an apparently "more correlated" spectrum. One first conclusion can thus be drawn: since unfolding reduces the first few channels (small values of t) of the $|FT|^2$, $\Sigma^2(L)$ is extremely sensitive to unfolding because it integrates $1 - b_2(t)$ between $0+$ and $t = 1/L$. On the contrary, $\Delta_3(L)$ is less sensitive to unfolding because the weighting function goes to zero when $t \to 0$.

The crucial question is now: what unfolding procedure is legitimate, that is, which $N_{av}(E)$ must be used to unfold the spectrum?

There is no well-defined answer except if we know the Hamiltonian (or the potential energy surface).[31] In any case each unfolding procedure can be seen as a high-pass filter that transforms $N(E)$ into $N_{fl}(E)$. Its cutoff frequency f_c prevents us from studying correlations at distances greater than $1/f_c$. For the vibronic levels of NO_2, and if the spectrum were complete, the dominant contribution of $N_{av}(E)$ would undoubtedly be "E^3" because it follows the law expected for the lower energy part of a three mode anharmonic oscillator. Now a question arises concerning Persch's spectrum: is this sinelike channel two component of the FFT real or spurious? We think that this modulation is due to missing levels. An explanation of this sinelike component could be due to a larger fraction of missing levels between 15 800 and 16 600 cm^{-1}, i.e., in the middle of Fig. 10. This interpretation is consistent with the absorption spectrum of Gillispie and Khan,[30] which shows a minimum of absorption in this energy range due to unfavorable bending Franck–Condon factors, leading naturally to more missing levels. In this case, fitting $N(E)$ with a more flexible $N_{av}(E)$ would be the best that could be done to unfold the spectrum in such a situation, but the counterpart is the "building-up" of spurious long range correlations. Note that no satisfactory solution can be found by playing with unfolding when the spectrum is incomplete: a more flexible $N_{av}(E)$ eliminates more low frequency components [small t in $1 - b_2(t)$], and eliminates that way any meaningful information that could be contained from these components.

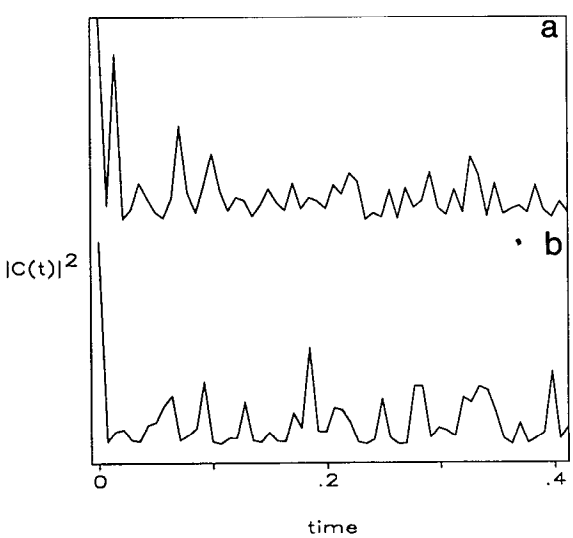

FIG. 15. $|FT|^2$ of the data of Persch *et al.* (Ref. 9) unsmoothed. (a) With $N_0 + a_3E^3 + a_6E^6$ unfolding: note the strong peak at channel two, which corresponds to the large oscillation at very low frequency of $N(E)$ around $N_{av}(E)$ (see Fig. 10). (b) With five variable knots spline unfolding: the strong peak at channel two has disappeared (see the text).

[1]T. A. Brody, J. Flores, J. B. French, P. A. Mello, A. Pandey, and S. S. M. Wong, Rev. Mod. Phys. **53**, 385 (1981).
[2]L. Leviandier, M. Lombardi, R. Jost, and J. P. Pique, Phys. Rev. Lett. **56**, 2449 (1986).
[3]E. Abramson, R. W. Field, D. Imre, K. K. Innes, and J. L. Kinsey, J. Chem. Phys. **80**, 2298 (1986).
[4]S. C. Farantos and J. Tennyson, NATO ASI Series C 1987, Vol. 200, pp. 15–30.
[5]R. Jost, A. Delon, and E. Pebay-Peyroula, Ber. Bunsenges. Phys. Chem. **92**, 412 (1988).
[6]K. Yamanouchi, S. Takeuchi, and S. Tsuchiya, J. Chem. Phys. **92**, 4044 (1990).
[7]E. Haller, H. Köppel, and L. S. Cederbaum, J. Mol. Spectrosc. **111**, 377 (1985).
[8]R. E. Smalley, L. Wharton, and D. H. Levy, J. Chem. Phys. **63**, 4977 (1975).
[9]G. Persch, E. Mehdizadeh, W. Demtröder, Th. Zimmermann, H. Köppel, and L. S. Cederbaum, Ber. Bunsenges. Phys. Chem. **92**, 312 (1988).
[10]G. Persch, H. J. Wedder, and W. Demtröder, J. Mol. Spectrosc. **123**, 356 (1987).
[11]C. F. Jackels and E. R. Davidson, J. Chem. Phys. **63**, 4672 (1975); **65**, 2941 (1976a); **64**, 2908 (1976b).
[12]G. D. Gillispie, A. V. Khan, A. C. Wahl, R. P. Hosteny, and M. Krauss, J. Chem. Phys. **63**, 3425 (1975).

[13]G. Hirsch and R. J. Buenker, Can. J. Chem. **63**, 1542 (1985); G. Hirsch, R. J. Buenker, and C. Petrongolo, Mol. Phys. **70**, 835 (1990).
[14]C. P. Blahous III, B. F. Yates, Y. Xie, and H. F. Schaefer III, J. Chem. Phys. **93**, 8105 (1990).
[15]A. Delon and R. Jost, J. Chem. Phys. **95**, 5686 (1991), preceding paper.
[16]S. Hiraoka, K. Shibuya, and K. Obi, J. Mol. Spectrosc. **126**, 427 (1987).
[17]E. Pebay-Peyroula, A. Delon, and R. Jost, J. Mol. Spectrosc. **132**, 123 (1988).
[18](a) See AIP Document No. PAPS JCPSA-95-5701-36 for 36 pages of the list of the 175 vibronic bands. Order by PAPS number and journal reference from American Institute of Physics, Physics Auxiliary Publication Service, 335 East 45th Street, New York, NY 10017. The price is $1.50 for each microfiche (98 pages) or $5.00 for photocopies of up to 30 pages, and $0.15 for each additional page over 30 pages. Airmail additional. Make checks payable to the American Institute of Physics. (b) Readers may refer to AIP Document No. PAPS JCPSA-95-5686-6 for 6 pages of the comparison between vibronic energies. Order by PAPS number and journal reference from American Institute of Physics, Physics Auxiliary Publication Service, 335 East 45th Street, New York, NY 10017. The price is $1.50 for each microfiche (98 pages) or $5.00 for photocopies of up to 30 pages, and $0.15 for each additional page over 30 pages. Airmail additional. Make checks payable to the American Institute of Physics.
[19]G. Persch, thesis, Kaiserlautern, Germany, 1987.
[20]H. Nagai, K. Shibuya, and K. Obi, J. Chem. Phys. **93**, 7656 (1990).
[21]E. Pebay-Peyroula, thesis, University of Grenoble, France, 1986.
[22]Th. Zimmermann, H. Köppel, L. S. Cederbaum, G. Persch, and W. Demtröder, Phys. Rev. Lett. **61**, 3 (1988).
[23]W. J. Lafferty and R. L. Sams, J. Mol. Spectrosc. **66**, 478 (1977).
[24]H. D. Bist and J. C. D. Brand, J. Mol. Spectrosc. **62**, 60 (1976).
[25]J. C. D. Brand, P. H. Chiu, and A. R. Hoy, Can. J. Phys. **57**, 428 (1979).
[26]K. Chen, G. P. Wang, C. Kuo, and C. Pei, Chem. Phys. **144**, 383 (1990).
[27]A. Delon, P. Dupré, and R. Jost (to be published).
[28]F. J. Dyson and M. L. Mehta, J. Math. Phys. **4**, 701 (1963).
[29]Th. Zimmermann, H. Köppel, and L. S. Cederbaum, J. Chem. Phys. **91**, 3934 (1989). See also E. Haller, H. Köppel, and L. S. Cederbaum, Chem. Phys. Lett. **101**, 215 (1983).
[30]G. D. Gillispie and A. V. Khan, J. Chem. Phys. **65**, 1624 (1976).
[31]L. D. Landau and E. M. Lifschitz, *Statistical Physics* (Pergamon, New York, 1969).
[32]R. A. Marcus and O. K. Rice, J. Phys. Colloid Chem. **55**, 894 (1951).
[33]I. Hamilton, J. Chem. Phys. **93**, 8081 (1990).
[34]M. L. Mehta, *Random Matrices and Statistical Theory of Levels* (Academic, New York, 1967).
[35]J. P. Pique, J. Opt. Soc. Am. B **7**, 1816 (1990).
[36]M. V. Berry, Proc. Roy. Soc. London, Ser. A **400**, 229 (1985).
[37]M. Lombardi, P. Labastie, M. C. Bordas, and M. Broyer, J. Chem. Phys. **89**, 3479 (1988).